University of Stuttgart
Germany

Faculty 6: Aerospace Engineering and Geodesy

Annual Report **2023**

Geodesy & Geoinformatics

IIG

G I S

INS

ifp

Dear friends and colleagues,

It is our great pleasure to present to you this annual report on the 2023 activities and academic highlights of the four institutes

- Institute of Geodesy (GIS),

- Institute for Photogrammetry and Geoinformatics (ifp),

- Institute of Navigation (INS),

- Institute of Engineering Geodesy (IIGS),

which contribute to the curricula of Geodesy and Geoinformatics at the University of Stuttgart and which are part of the Faculty of Aerospace Engineering and Geodesy.

Preface

Global and local political developments in 2023 had also had a strong impact on the way how we carry out our research and education. Risen prices, the shortage of skilled workers as well as limitations in access to components posed several challenges, which were not impossible to be overcome, but surely took us a lot of time. Nevertheless, it can be stated that all institutes had still a very prosperous year in their research work. It was possible to establish new collaborations or attract new undergraduate and graduate students. Thus, we can surely say that we were able to further increase the visibility of Geodesy and Geoinformatics on national and international levels.

Research

This annual report documents our research contributions in many diverse fields of Geodesy and Geoinformatics: from satellite and physical geodesy through navigation, remote sensing, engineering surveying and telematics to photogrammetry, geographical information systems and location based services. Detailed information on projects and research output can be found in the following individual institutes' sections.

Teaching

We were able to welcome 16 new BSc students in winter term 2023/2024. For the first semester of the MSc program for Geodesy and Geoinformatics we welcomed 4. Please visit our website

www.geodaesie.uni-stuttgart.de

or check our Instagram account

https://www.instagram.com/geodaesie_stuttgart/

for additional information on the programs.

Our successful international MSc program Geomatics Engineering (GeoEngine) exists already 18 years. Probably due establishment of tuition fees for non-EU students in 2018, we saw a decline of new students since then. We welcomed only 14 students in 2023. In order to address this issue, we have completely revised the GeoEngine curriculum so that, in the end, we created a new international master program, named "Geomatics for Environmental Monitoring (GEM)", from which we hope that it will increase the interest in studying with us.

Awards and Scholarships

We want to express our gratitude to our friends and sponsors, most notably:

- Verein Freunde des Studienganges Geodäsie und Geoinformatik an der Universität Stuttgart e.V. (F2GeoS),
- Ingenieur-Gesellschaft für Interfaces mbH (IGI),
- DVW Landesverein Baden-Württemberg,

who support our programs and our students with scholarships, awards and travel support. Below is the list of the recipients of the 2023 awards and scholarships. The criterion for all prizes is academic performance; for some prizes GPA-based, for other prizes based on thesis work. Congratulations to all recipients!

Award	Recipient	Sponsor	Programme
Karl-Ramsayer Preis	Mr. Hannes Nübel	Department of Geodesy & Geoinformatics	Geodesy & Geoinformatics
BSc Thesis Award	Mr. Jiaxin Liu	F2GeoS	Geodesy & Geoinformatics
MSc Thesis Award	Mr. Yuke Xie	F2GeoS	Geodesy & Geoinformatics

Thomas Hobinger, Associate Dean (Academic)

thomas.hobiger@ins.uni-stuttgart.de

Institute of Engineering Geodesy

Geschwister-Scholl-Str. 24 D
70174 Stuttgart
Germany
Tel.: +49 711 685 84041
Fax: +49 711 685 84044
sekretariat@iigs.uni-stuttgart.de or
firstname.secondname@iigs.uni-stuttgart.de
http://https://www.iigs.uni-stuttgart.de/

Head of Institute

Prof. Dr.-Ing. habil. Dr. h.c. Volker Schwieger

Secretary

Elke Rawe
Désirée Schreib

Scientific Staff

M.Sc. Laura Balangé	Quality Modeling
Dipl.-Ing. Lyudmila Gorokhova	Kinematic Positioning
Dr.-Ing. Gabriel Kerekes	Terrestrial Laser Scanning
M.Sc. Philipp Luz	Digital Map
Dr.-Ing. Martin Metzner	Engineering Geodesy
M.Sc. Christoph Sebald	GIS for Climate Data
M.Sc. Ronja Miehling (since 01.01.2023)	Robotic Total Station
Dr.-Ing. Li Zhang	Engineering Geodesy
Ph.D. Stanislav Shevchuk (since 01.09.2023)	GNSS, Map Matching

Technical Staff

Dipl.-Ing. (FH) Andreas Kanzler (until 30.09.2023)
Martin Knihs, Mechanikermeister
Dipl.-Geogr. Lars Plate

External Teaching Staff

Dipl.-Ing. Jürgen Eisenmann	Landesamt für Geoinformation und Landentwicklung, Abteilungsleiter Flurneuordnung, Liegenschaftskataster
Dr.-Ing. Frank Friesecke	Prokurist der STEG Stadtentwicklung GmbH
Dipl.-Ing. Jonas Stadler	Landratsamt Alb-Donau-Kreis Fachdienst Flurneuordnung
Dipl.-Math. Ulrich Völter	Geschäftsführer der Fa. Intermetric
Dr.-Ing. Thomas Wiltschko	Daimler AG, Mercedes-Benz Cars; Research and Development

PhD-Students

M.Sc. Julia Aichinger	Terrestrial Laser Scanning
Dipl.-Ing. Patric Hindenberger	Location Referencing
M.Sc. Yu Li	Digital Map
M.Sc. Annette Schmitt	Multi-Sensor-Systems
M.Sc. Tobias Schröder	Automation of Production Process
M.Sc. Yihui Yang	Multi-Sensor-Systems
M.Sc. Christian Bader	Kinematic Laser Scanning

IntCDC Guest Professor

Prof. Dr. Andreas Wieser (ETH Zürich) (June/July 2023)

General View

The Institute of Engineering Geodesy (IIGS) is directed by Prof. Dr.-Ing. habil. Dr. h.c. Volker Schwieger. It is part of Faculty 6 "Aerospace Engineering and Geodesy" within the University of Stuttgart. Prof. Schwieger holds the chair in "Engineering Geodesy and Geodetic Measurements".

In addition to being a member of Faculty 6, Prof. Schwieger is co-opted to Faculty 2 "Civil and Environmental Engineering". Furthermore, the IIGS is involved in the Center for Transportation Research of the University of Stuttgart (FOVUS). Thus, the IIGS actively continues the close collaboration with all institutes in the field of transportation, especially with those belonging to Faculty 2.

Since 2011, Prof. Schwieger is a full member of the German Geodetic Commission (Deutsche Geodätische Kommission – DGK). Furthermore, he is head of the section "Engineering Geodesy" within the DGK since 2020.

The institute's main tasks in education focus on geodetic and industrial measurement techniques, kinematic positioning and multi-sensor systems, statistics and error theory, engineering geodesy and monitoring, GIS-based data acquisition, and geo-mobility. The IIGS

is responsible for the above-mentioned fields within the curricula of "Geodesy and Geoinformatics" (Master and Bachelor in German) and for "GeoEngine" (Master for Geomatics Engineering in English). In addition, the IIGS provides several courses in German for the curricula of "Aerospace Engineering" (Bachelor and Master), "Civil Engineering" (Bachelor and Master), "Transport Engineering" (Bachelor and Master) and "Technique and Economy of Real Estate" (Bachelor and Master). Furthermore, lectures are given in English to students within the Master course "Infrastructure Planning". The cluster "Integrative Computational Design and Construction for Architecture" (IntCDC), for which the University of Stuttgart had submitted a funding application as part of the excellence strategy to strengthen cutting-edge research in Germany, was awarded funding for 2019 to 2025. The cluster IntCDC aims to harness the full potential of digital technologies in order to rethink design and construction, and enable ground breaking innovations for the building sector through a systematic, holistic, and integrative computational approach. As a member of the cluster (IntCDC), the institute's research in the field of new construction methods is intensified in cooperation with architects, civil engineers, computer scientists, production engineers, social scientists, and other scientists from various research institutions within and outside the University of Stuttgart.

The research and project work of the institute is expressed in the course contents, thus always presenting the current state-of-the-art to the students. As a benefit of this, student research projects and theses are often implemented in close cooperation with the industry and external research partners. The main research focuses on kinematic and static positioning, analysis of engineering surveying processes and construction processes, machine and robot guidance, monitoring, geo-mobility, process and quality modeling. The daily work is characterized by intensive co-operation with other engineering disciplines, especially with traffic engineering, civil engineering, architecture, and aerospace engineering.

Research and Development

AI-supported Collaborative Control and Trajectory Generation of Mobile Manipulators for Indoor Construction Tasks

To initiate positioning and tracking, the IIGS established a network of fixed points evenly distributed in the Large-Scale Construction Robotics Laboratory (LCRL). The coordinates as well as the accuracies of the fixed points were calculated. A prism was mounted on the sensing robot and its position can be determined with a total station.

As the total station does not operate under the Robot Operating System (ROS), the hardware and software requirements for the communication between the total station and the sensing robot were provided. As a result, the total station is integreted in the ROS and receives the timestamp from the common time server, allowing it to be synchronized with the other sensors. To take advantage of all sensor measurements, a three-dimensional error state Kalman filter was implemented in RP 26-1.

This filter estimates not only the position, velocity and orientation of the sensing robot, but also the biases of the accelerometer and gyroscope sensors. The results were compared to the absolute positions from the total station and later to the Simultaneous Localization and Mapping (SLAM) results. The next step would be the real-time integration of the Kalman filter and the SLAM.

Besides positioing, the generation of a digital twin components is the task of RP 26-1. As the planned construction is already represented as a "Buildings and Habitats object Model" (BHoM) by the colleagues in RP 9-2, the IIGS focused on static terrestrial laser scanning to evaluate the as-built geometry. Using the Trimble X7 laser scanner, a total of 103 scans were carried out at different locations indoors and outdoors. This was followed by an offline processing of the point clouds including registration, georeferencing, segmentation, modeling and classification with the two programs Trimble RealWorks and BricsCAD. The required object classes were derived from the BHoM provided by RP 9-2. Finally, a BIM model was created and exported in the standard IFC format. The provided geometry will be used as a reference to evaluate the geometry from SLAM.
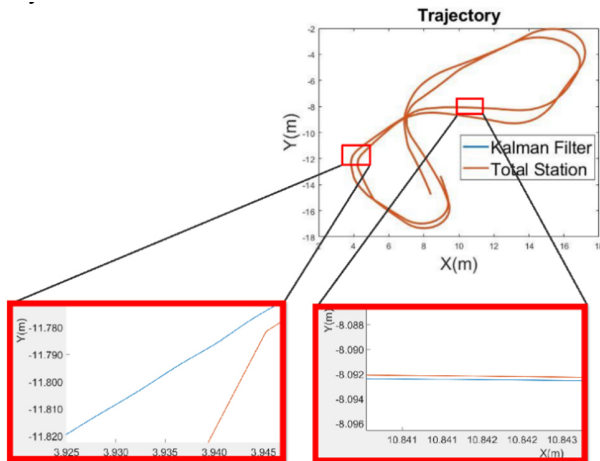

Figure 1: Comparison of the Kalman filter trajectory with the total station trajectory

Holistic Quality Model for Extension of Existing Buildings

Within the Cluster of Excellence "Integrative Computational Design and Construction for Architecture" (IntCDC), the RP18-2 "Holistic Quality Model for Extension of Existing Buildings" deals with the development of a holistic quality model for existing buildings. This is being done in close collaboration with the Institute for Acoustics and Building Physics (IABP) for environmental quality, the Institute for Social Sciences (SOWI) for social quality and the Institute for Construction Management (IBL). The aim of the IIGS is to analyze the technical quality.

In collaboration with our project partners, we have developed a method to describe the interrelations between the individual disciplines and thus being able to represent them also numerically. Another focus of the joint work was the development of a concept to identify the individual phases of construction in existing buildings and to identify the control and decision points in the planning process.

The disciplinary research in the project also focused on quality assurance in the area of fiber composite systems. In order to determine the geometric quality of structures made of fiber composite systems, the position of the individual fibers and their intersections must be known. The following algorithm was developed to determine the fibers and their intersections. First, the component is digitized using a terrestrial laser scanner. The result is a point cloud. This is divided into clusters for further processing. The k-means clustering method is used for this. An iterative Hough transformation is then used to search for lines in each cluster. Subsequently, incorrect lines are filtered. Various criteria are applied here. Among other things, the fiber thickness, the number of points per line and the parallelism of lines are taken into account. Next, the intersections between the individual lines are calculated and checked for correctness. Finally, the lines and intersections found for all clusters are combined. The algorithm is transferable to different data sets. The accuracy varies greatly depending on the quality of the point cloud and the complexity of the building object.

Figure 2: Result of segmentation and line estimation with two examples

In addition to determining the geometry, investigations have also been carried out in the area of analyzing measurement uncertainties, as a result of the measured material in order to be able to take these into account in the quality assessment.

Cyber-Physical On-Site Construction Processes Using a Spider Crane Robotic Platform

As a part of the Cluster of Excellence IntCDC, the RP16-2 deals with the further improvement of the already developed cyber-physical construction (CPC) instrumentation platform. Based on the general project idea of using two robotic cranes in co-operation with each other for automated assembly, the current development focuses on a single robotic spider crane.

The actual second phase of the project was launched in July 2022. The potential of using cameras integrated directly into image-assisted robotic total stations (IATS) was considered as a main research point. In this case, the focus of interest is not the crane itself, but the construction part that is moved by the crane. Following the project life cycle (see Figure 3), the first step was to apply the previously developed calibration procedure in relation to 5 IATS Trimble S7 involved in the project, in order to empirically confirm the difference between the cross-hair target point (optical axis of the telescope) and the camera center. The results of the calibration functions obtained are shown in Figure 4.
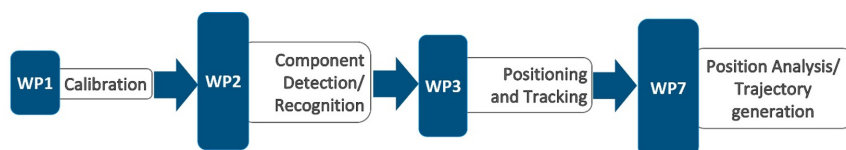

Figure 3: Project Life Cycle

Afterwards, the original aim of camera calibration was extended to the evaluation of the existing results by developing a mathematical model for the correct conversion between the camera coordinate system and the coordinate system of the IATS. This step is currently under development. In addition, initial studies on the correct algorithms for object detection and tracking have been carried out, together with setting up the correct workflow for data and video streaming between IATS and PC. The new Trimble Ri coaxial robotic total station is being tested as part of the hardware upgrade.

Last but not least, coming back to the spider crane itself, a series of precise measurements were performed using a laser tracker to determine the position of the fixed points on the crane surface that are used for orientation in the zero position before each start. Here, two main tasks are covered: the quality control of the construction of the robotic crane itself and the control of the alignment of the internal crane axis for the correct coordinate transformation between the crane coordinate system and the IATS coordinate system.
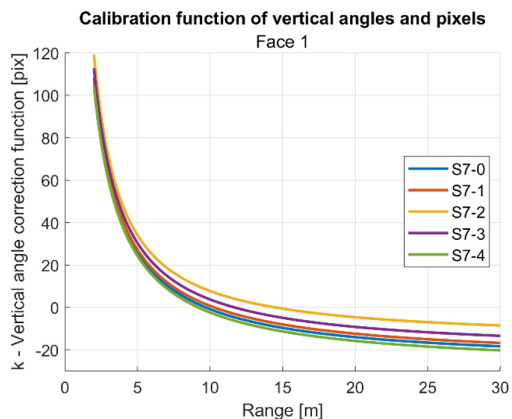
Calibration function of vertical angles and pixels

Face 1

Figure 4: Example of the calibration functions for IATS Trimble S7

Scanning the BioMat 3DNaturDruck at TIME SPACE EXISTENCE in Venice 2023

Continuing the line of successful cooperation between the Institute of Engineering Geodesy (IIGS) and the Institute of Building Structures and Structural Design (ITKE), last year's scanning task took place in one of the most famous cities in the world, Venice.

The BioMat Department of ITKE participated in the Venice Architecture Biennale 2023, as part of the Biennale collateral event entitled TIME SPACE EXISTENCE, organized by the European Cultural Center (ECC). Among the three recent projects advancing the application of biomaterials is a demonstrator called 3DNaturDruck, which explores the architectural application of 3D-printed natural fibers. Through interdisciplinary research, this project aims to co-design a new materialization process by interconnecting the fields of architectural design, engineering and digital fabrication. The column demonstrator "Ligno Print" (Figure 5) represents a viable strategy for the application of this emerging material method in large-scale architectural scenarios, a new territory for this particular natural fiber technique.

The task of the IIGS was to capture the as-built geometry of the Ligno Print in Venice and later to verify the manufacturing (printing) quality of the construction components. Currently, the data is being processed with the aim of detecting the components that deviate from the originally designed geometry during the manufacturing process (Figure 5).
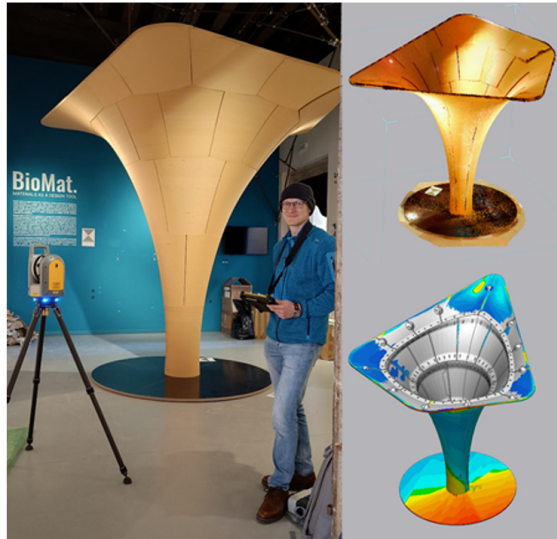
Figure 5: Left: scanning the BioMat Lingo Print pavilion; Right: point cloud and comparison with 3D model used for printing the 3D parts

Towards the extrinsic Synchronization of Observations Acquired with a Network of Robotic Total Stations

High-precision positioning in real time is a crucial aspect of automation in the construction industry. One way to provide absolute positions in real time is to use robotic total stations (RTSs). In addition to providing redundancy in positioning, RTS networks can help to ensure the uninterrupted flow of the automated process. This can only be achieved if a common temporal and spatial frame is available for all the RTSs in the network. In 2023, an approach for synchronizing observations from an RTS network was developed at the IIGS. Four Trimble S7 RTSs were used in this network and the time frame was provided by an NTP server (Figure 6). The possibilities for synchronizing observations streamed at 10 Hz and at 20 Hz were tested using reflectors mounted on a rotating arm. Different scenarios with angles in combination with distance measurements and pure angle measurements are presented.

The achieved simultaneity is about 0.3 ms between sole angle measurements from four individual RTS streaming data at 10 Hz. In reality, however, only measurements with a sampling rate of 5 Hz are available for the time being, and streaming at higher rates leads to duplicated values. Simultaneity in tracking mode remains a challenge due to the randomness of the initial measurements. Although the measurements are triggered at the same time, each RTS starts tracking at slightly different times. Delays can reach up to more than 150 ms in the current setup.

The achieved geometric quality was asserted using moving objects at constant speeds. The tests involved reflectors on a rotation arm at speeds of 0.66 m/s ($\sim$2.4 km/h) with a precisely known reference geometry determined by laser tracker. Based on individual RTS measurements in tracking mode, RMS values of less than 5 mm were obtained. If outliers are eliminated, the average RMS value drops at 2 mm.
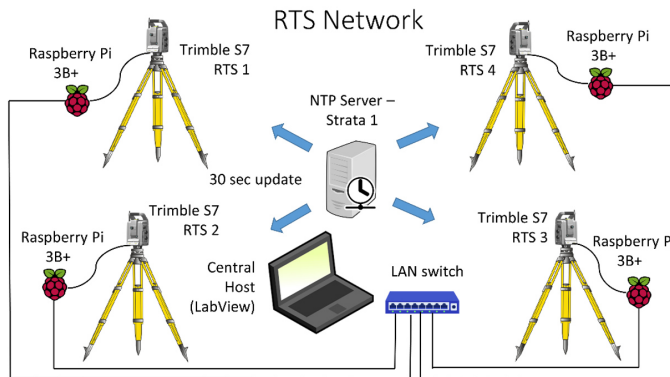

Figure 6: System overview of the RTS network realized at the IIGS within IntCDC

ConMoRAIL

The aim of the ConMoRAIL project is to develop a monitoring system which is cost-effective, board-autonomous and permit-free, meaning it should not require special authorization from the German railway regulatory authorities to be installed and used during regular service. This system is intended to precisely locate and detect certain track faults while driving in regular service, and save detected faults in a database that can be used to facilitate mainte-nance of these tracks. This project is conducted in cooperation with the Institute of Railway and Transportation Engineering (IEV) at the University of Stuttgart and the Württembergische Eisenbahn-Gesellschaft (WEG).

The localization program is a key component of the monitoring system. This program is designed to precisely locate the train vehicle using GNSS and IMU measurements. These measurements will be used in a sensor fusion algorithm to combine the data and thus calculate precise locations of the train. To further refine the algorithm, underlying map data from OSM (Open Street Maps) will be integrated. As the system is designed to record track data continuously, existing data from the map as well as track faults can be validated and refined to obtain a more accurate representation of the current track conditions. The resulting map can then be used to schedule maintenance work according to the conditions.

First tests were conducted to obtain initial data and to establish the requirements needed for the sensor configuration. This data is also analyzed to detect critical sections that need further investigation.

The project is funded by the DFG (German Research Foundation) under the project number 515687155.

Figure 7: Recorded track data

Ghosthunter III

The aim of the Ghosthunter III project is to develop an app for Android smartphones that will help to reliably detect wrong-way drivers on freeways and their ramps, and to warn the wrong-way drivers themselves as well as the other road users in the surroundings. This project is carried out in cooperation with the Institute of Space Technology and Space Applications at the University of the Federal Armed Forces Munich and with the company NavCert GmbH.

Supported by:

Federal Ministry for Economic Affairs and Climate Action

on the basis of a decision by the German Bundestag

In the course of the project, the developed application had to be tested for its false alarm rate and sensitivity. Due to the large number of highway entries driven per day in Germany, a correspondingly large sample ($n > 4 \cdot 10^8$) must be selected in order to be able to make a significant statement. To test the application with such a large number of trajectories, a simulator was developed that can simulate freeway entrances throughout Germany. Based on a digital map, error models for GNSS and map errors, this simulator generates trajectories that are then examined by the app's algorithms for wrong-way drivers, and the results thereof are statistically evaluated. The simulator was also used to compare different application parameters.

In its final version, the application achieved a false alarm rate of $6.7 \cdot 10^{-5}$ and a sensitivity of 0.72. The research project Ghosthunter III is granted by the German Federal Ministry of Economic Affairs and Energy (BMWi) and the German Aerospace Center (DLR) under grant number 50 NA 2109.

Figure 8: Ghosthunter app for wrong-way driver detection.

CoKLIMAx

The CoKLIMAx project started in November 2021. It deals with the use of COPERNICUS climate data for climate-relevant urban planning. Throughout 2023, while the project partners from GERICS, HTWG and the City of Constance made increasing use of the available applications on the ArcGIS Enterprise 10.9.1 platform in the CODE-DE cloud environment, the backend setup as well as configuration and fine-tuning continued. In autumn 2023, the whole system started to run smoothly due to regular reviews and update checks. The work was mostly carried out with the support of external IT-staff from CODE-DE and Baral Geohaus-Consulting.

Meanwhile, a number of data-pull and other extract, transform, and load (ETL) processes were developed to derive and process data from the Climate Data Store (CDS), and other sources. Content for the Advanced Municipal Climate Data Store toolbox (AMCDS Toolbox) became visible. For instance, the workflow and vegetation-health-dashboard (Figure 9) was developed, an accompanying paper published.

In April 2023, a preparatory toolbox-workshop in and with the city of Constance took place in preparation for the AMCDS toolbox developed. On 15 June 2023 the Baral Connect 2023 conference took place in the City Hall of Reutlingen, where the project was presented. On 5 October, the CoKLIMAx project team presented the first results to employees of the city of Constance.

Figure 9: Workflow and vegetation-health-dashboard

Representatives of different departments (e.g., Civil Engineering Department, Office for Urban Planning and Environment, Waste Management, Office of Property and GIS) took an active part in the workshop. In late November 2023, the project was presented at the ESRI Germany Conference, which took place at the World Conference Center in Bonn.

Last but not least, on 5 December 2023, the paper entitled "Modelling Vegetation Health and Its Relation to Climate Conditions Using Copernicus Data in the City of Constance" was submitted to MDPI Remote Sensing and later on published. The focus was on the state (health) of the vegetation and its response to climate conditions. This is crucial for assessing the impact of climate change on the urban environment. The results are intended to help generate new insights and improve resilient, climate-friendly urban planning by providing an intuitive tool for monitoring plant health and its response to climate conditions.

The CoKLIMAx research project is funded by the German Federal Ministry for Digital and Transport (BMDV) and the German Aerospace Center (DLR) as part of the "Climate Adaptation Strategies for Municipal Applications in Germany" under grant number 50EW2103C.
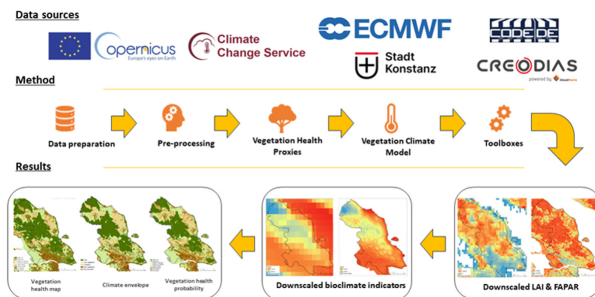

Figure 10: Modelling Vegetation Health and Its Relation to Climate Conditions Using Copernicus Data in the City of Constance

Studies on Deformation Analysis of TLS Point Clouds using B-splines

For the modeling of terrestrial laser scan data using B-spline surfaces, mainly methods for the estimation of surface parameters are currently used. A new approach is the direct use of 3D laser scan data as control points, and a mapping algorithm of two epochs using a curvature parameter. The mapping algorithm is used to identify identical points in both epochs in order to transform both epochs into a common coordinate system. The Boehm knot insertion algorithm was implemented as a base to ensure the filling of control points in the control grid of the tensor product B-spline surface to be generated, without changing the shape of the B-spline surface.

The developed mapping algorithm consists of two steps, which are divided into coarse and fine mapping. In the coarse mapping, the curvature parameters of both epochs are superimposed and shifted as a grid in rough steps. The shift position with the highest value of the correlation coefficient provides the basis for defining the procedure in step two of the mapping algorithm, the fine mapping. Figure 11 shows the evaluation of the correlation coefficients in the first step of the mapping algorithm for a laser scan test specimen. The results of this correlation analysis provide the base for defining identical points in two epochs of laser scan data. This has to be done in order to transform one epoch into the coordinate system of the other by means of 6-parameter transformation, and to ensure a direct coordinate comparison of two associated B-spline surface points for identifying possible deformations.
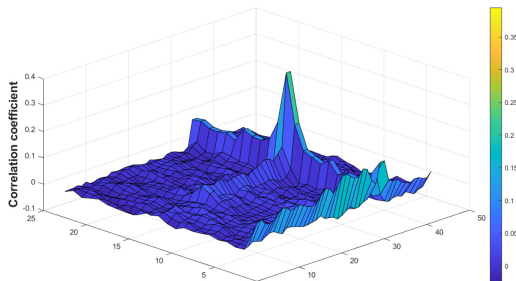

Figure 11: Correlation coefficients of the mapping algorithm of a test specimen

Driving Environment Inference from POI of Navigation Map: Fuzzy Logic and Machine Learning Approaches

To adapt vehicle control and plan strategies in a predictive manner, it is usually desired to know the context of a driving environment. This project aims at efficiently inferring the following five driving environments around vehicle's vicinity: shopping zone, tourist zone, public station, motor service area, and security zone, whose existences are not necessarily mutually exclusive. To achieve that, we utilize the Point of Interest (POI) data from a navigation map as the semantic clue, and solve the inference task as a multilabel classification problem. Specifically, we first extract all relevant POI objects from a map, then transform these discrete

POI objects into numerical POI features. Based on these POI features, we finally predict the occurrence of each driving environment via an inference engine. To calculate representative POI features, a statistical approach is introduced. To composite an inference engine, three inference systems are investigated: fuzzy inference system (FIS), support vector machine (SVM), and multilayer perceptron (MLP). In total, we implement 11 variants of inference engines following two inference strategies: independent and unified inference strategies, and conduct comprehensive evaluation on a manually collected dataset. The result shows that the proposed inference framework generalizes well on different inference systems, where the best overall F1 score 0.8699 is achieved by the MLP-based inference engine following the unified inference strategy, along with the fastest inference time of 0.0002 millisecond per sample. Hence, the generalization ability and efficiency of the proposed inference framework are proved.

Figure 12 illustrates the target of this project, and Figure 13 depicts the overview of the proposed inference framework. For further details please refer to our publication (Yu et al. 2023).

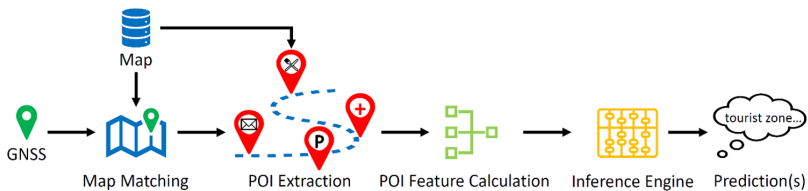Figure 12: Using POI for driving environment inference

Figure 13: Overview of the proposed inference framework

Advanced Automated Gap and Flush Measurement assisted by a Highly Flexible and Accurate Robotic System

Quality is a crucial factor in the automotive industry, as it can make or break a company's reputation and success in the global market. With increasing competition and consumer demands for high-quality vehicles, manufacturers are constantly seeking ways to improve their production processes and ensure that their products meet the highest standards of quality and safety.

One important aspect of quality control in vehicle production is gap and flush measurement. This involves measuring the gaps and transitions between different parts of the vehicle, such as the doors, hood, and trunk, to ensure that they are within specified tolerances and that the vehicle is both aesthetically pleasing and functional. To achieve this, automated gap measurement systems are used, which employ lightweight robots and mobile robot platforms to measure entire finished vehicles quickly and accurately.

In addition to gap and transition measurement, other factors that contribute to the overall quality of a vehicle include reliability, completeness, occupational safety, efficiency, accuracy, and timeliness. These factors are closely monitored throughout the production process to ensure that the final product meets the highest standards of quality and safety. These factors are the main factors of the quality model that was designed to improve the measurement system.

Another area where quality is becoming increasingly important is in the development of large language models (LLMs) for chatbots and other applications. With the growing use of chatbots in various environments, it is essential to ensure that these systems are reliable, accurate, and secure. To achieve this, a test suite is being developed that includes various metrics to evaluate the performance of LLMs, including their response to adversarial attacks, factuality, and dodging.

To optimize the performance of the test suite, a judge is used to evaluate the LLM's responses and provide feedback on areas for improvement. However, training and optimizing the judges is a significant challenge, as it requires extensive test and training data for each metric. Nonetheless, the development of a robust test suite including the judges is essential to ensure that LLMs and other chatbots are reliable and accurate, and that they meet the highest standards of quality and security.

PhD Seminar

The 14th Doctoral Seminar of the Engineering Geodesy Section of the DGK was organized by the Institute of Geodesy and Photogrammetry at the ETH Zürich. A total of 11 presentations mirrored the work of PhD candidates from Poland, Austria, Switzerland, and Germany. Fruitful discussions between the 90 participants were possible during the coffee breaks and in the evening at the highly anticipated get-together. After the successful participation of the IIGS members with contributions from Philipp Luz and Yu Li, a long bus ride back to Stuttgart crowned the experience.

Publications

Refereed Publications

Abdallah, A., Agag, T., & Schwieger, V. (2023). Method of Development of a New Regional Ionosphere Model (RIM) to Improve Static Single-Frequency Precise Point Positioning (SF-PPP) for Egypt Using Bernese GNSS Software. Remote Sensing, 15(12), Article 12. https://doi.org/10.3390/rs15123147

Balangé, L., Sprügel, N., & Schwieger, V. (2023). Segmentierung und Modellierung von Fasern für die Qualitätssicherung von Faserverbundsystembauteilen mittels terrestrischem Laserscanning. In A. Wieser (Hrsg.), Beiträge zum 20. Internationalen Ingenieurvermessungskurs Zürich 2023. Wichmann VDE Verlag, Berlin. https://www.vde-verlag.de/buecher/537734/ingenieurvermessung-23.html

Gil Pérez, M., Mindermann, P., Zechmeister, C., Forster, D., Guo, Y., Hügle, S., Kannenberg, F., Balangé, L., Schwieger, V., Middendorf, P., Bischoff, M., Menges, A., Gresser, G. T., & Knippers, J. (2023). Data processing, analysis, and evaluation methods for co-design of coreless filament-wound building systems. Journal of Computational Design and Engineering, 10(4), Article 4. https://doi.org/10.1093/jcde/qwad064

Haala, N., Zhang, W., Joachim, L., Skuddis, D., Abolhasani, S., Schwieger, V., & Sörgel, U. (2023). On the Potential of SLAM Approaches for Real-time Geodetic Measurement Tasks. AVN - Allgemeine Vermessungsnachrichten, Wichmann Verlag, 5 2023

Kerekes, G., & Schwieger, V. (2023). An approach for considering the object surface properties in aTLS stochastic model. Journal of Applied Geodesy. https://doi.org/doi:10.1515/jag-2022-0032

Lauer, A. P. R., Benner, E., Stark, T., Klassen, S., Abolhasani, S., Schroth, L., Gienger, A., Wagner, H. J., Schwieger, V., Menges, A., & Sawodny, O. (2023). Automated on-site assembly of timber buildings on the example of a biomimetic shell. Automation in Construction, 156, 105118 https://doi.org/10.1016/j.autcon.2023.105118

Lauer, A. P. R., Lerke, O., Blagojevic, B., Schwieger, V., & Sawodny, O. (2023). Tool center point control of a large-scale manipulator using absolute position feedback. Control Engineering Practice, 131, 105388. https://doi.org/10.1016/j.conengprac.2022.105388

Lauer, A. P. R., Lerke, O., Gienger, A., Schwieger, V., & Sawodny, O. (2023). State Estimation with Static Displacement Compensation for Large-Scale Manipulators. SII Atlanta.

Li, Y., Metzner, M., & Schwieger, V. (2023). Driving Environment Inference from POI of Navigation Map: Fuzzy Logic and Machine Learning Approaches. Sensors, 23(22), Article 22. https://doi.org/10.3390/s23229156

Yang, Y., & Schwieger, V. (2023). Patch-based M3C2: Towards lower-uncertainty and higher-resolution deformation analysis of 3D point clouds. International

Journal of Applied Earth Observation and Geoinformation, 125, 103535. https://doi.org/10.1016/j.jag.2023.103535

Yang, Y., & Schwieger, V. (2023). Supervoxel-based targetless registration and identification of stable areas for deformed point clouds. Journal of Applied Geodesy, 17(2), Article 2 https://doi.org/doi:10.1515/jag-2022-0031.

Non-Refereed Publications

Zhang, L., Balangé, L., & Schwieger, V. (2023). Geometric Quality Assurance within the Research Cluster IntCDC. FIG Working Week 2023, Orlando, USA. https://fig.net/resources/proceedings/fig_proceedings/fig2023/papers/pe_01/PE_01_zhang_balange_et_al_12021.pdf

Publication of Dataset

Gil Pérez, M., Mindermann, P., Zechmeister, C., Forster, D., Guo, Y., Hügle, S., Kannenberg, F., Balangé, L., Schwieger, V., Middendorf, P., Bischoff, M., Menges, A., Gresser, G. T., & Knippers, J. (2023). Post-processed and normalized data sets for the data processing, analysis, and evaluation methods for co-design of coreless filament-wound structures. DaRUS. https://doi.org/10.18419/darus-3449

Gil Pérez, M., Zechmeister, C., Kannenberg, F., Mindermann, P., Balangé, L., Guo, Y., Hügle, S., Gienger, A., Forster, D., Bischoff, M., Tarín, C., Middendorf, P., Schwieger, V., Gresser, G. T., Menges, A., & Knippers, J. (2023). Object model data sets of the case study specimens for the computational co-design framework for coreless wound fibre-polymer composite structures. DaRUS. https://doi.org/10.18419/darus-3375

Presentations

Abolhasani, S.: Echtzeittachymeternetz zur Robotersteuerung, 13. Jenaer GeoMessdiskurs 2023, 29.06.2023, Jena.

Balangé, L., Di Bari, R., Bornschlegl. S. Haag, P.: RP18-2: Holistic Quality Model (HQM) for extension of existing buildings: social, environmental, technical and economic integration Holistic Quality Model, Research Network Colloquium 2023, 03.03.2023, Stuttgart.

Balangé, L.: Segmentierung und Modellierung von Fasern für die Qualitätssicherung von Faserverbundsystembauteilen mittels terrestrischem Laserscanning. 20. Internationalen Ingenieurvermessungskurs, 11.-14.04.2023, Zürich 2023.

Hierholz, A., Reß, V., Abolhasani, S.: RP26-1: AI-supported Collaborative Control and Trajectory Generation of Mobile Manipulators for Indoor Construction Tasks, Research Network Colloquium 2023, 03.03.2023, Stuttgart.

Hierholz, A., Sörgel, U., Abolhasani, S.: RP26-1: AI-supported Collaborative Control and Trajectory Generation of Mobile Manipulators for Indoor Construction Tasks, Status Seminar 2023, 16.-17.11.2023, Bad Boll.

Gorokhova, L.: Camera calibration and alignment of optic axes for image-based robotic total station. XVI International Science and Technology Conference. Current Problems in Engineering Surveying. 21-22.09.2023. Poznan, Poland

Kerekes, G.: Omul – măsura lucrurilor, Smart Diaspora Geomatica 2023, Timisoara, 10.-13.04.2023, Romania.

Kerekes, G.: Stochastische Modellierung für TLS mittels des Elementarfehlermodells, DVW Seminar Next Level TLS – neue Verfahren und praxisnahe Einblicke! 04.-05.12.2023. Fulda, Germany

Lauer, A., Gong, Y., Gorokhova, L.: RP16-2: Cyber-Physical On-Site Construction Processes Using a Spider Crane Robotic Platform, Research Network Colloquium 2023, 03.03.2023, Stuttgart.

Lauer, A., Gong, Y., Gorokhova, L.: RP16-2: Cyber-Physical On-Site Construction Processes Using a Spider Crane Robotic Platform, Status Seminar 2023, 16.-17.11.2023, Bad Boll.

Li, Y.: Map-supported Road Boundary Detection and Tracking using LiDAR Sensor. DGK PhD Seminar ETH Zürich, 09.11.2023, Zürich, Switzerland.

Luz, P.: Automatic generation of a lane-level resolution road map from OSM data and its application in lane-level navigation, DGK PhD Seminar ETH Zürich, 09.11.2023, Zürich, Switzerland.

Schwieger, V.: Ingenieurgeodätische Beiträge in IntCDC. DVW Fachtagung. 17.05.2023, Stuttgart.

Schwieger, V.: Engineering Geodesy for Integrative Computational Design and Construction. XVI International Science and Technology Conference. Current Problems in Engineering Surveying. 21-22.09.2023. Poznan, Poland

Schwieger, V.: Positioning and Control of Construction Machines and Robots, Quality Control in Construction, Research at IIGS. Lectures at Technical University of Civil Engineering Bucharest, Romania, 24./25.10.2023

Schwieger, V.: Engineering Geodesy for Integrative Computational Design and Construction. 6th Conference of the UTCB Doctoral School, Bucharest, Romania, 26.10.2023

Schwieger, V.: Vorstellung der Abteilung Ingenieurgeodäsie, Jahressitzung des Ausschusses Geodäsie (DGK), München, 22.-24.11.2023

Sebald, C.: Nutzung von COPERNICUS Daten zur klimaresilienten Stadtplanung am Beispiel von Wärme, Wasser & Vegetation, Baral Connect 2023 - Mit GIS in die Zukunft, Präsentation, 15.06.2023, Reutlingen, Germany.

Sebald, C.: Nutzung von COPERNICUS Daten zur klimaresilienten Stadtplanung am Beispiel von Wärme, Wasser & Vegetation, 2nd CoKLIMAx Consortium Meeting with Urban-GreenEye, 28. – 29.09. 2023, City Hall -Leipzig, Germany.

Sebald, C.: CoKLIMAx: Mit Copernicus-Daten zur klimaresilienten Stadtplanung, ESRI Kon 2023, Special Interest Groups - Imagery, 29 - 30 11.2023, World Conference Center Bonn, Germany.

Zhang, L.: Geometric Quality Assurance within the Research Cluster IntCDC. FIG Working Week 2023, Orlando, USA.

Activities at the University and in National and International Organizations

Volker Schwieger

Full member of the German Geodetic Commission (Deutsche Geodätische Kommission – DGK)

Head of the section "Engineering Geodesy" within the German Geodetic Commission (DGK)

Chief Editor of Peer Review Processes for FIG Working Weeks and Congresses

Member of the Editorial Board "Journal of Applied Geodesy"

Member of the Editorial Board "Journal of Applied Engineering Science"

Member of the Editorial Board "Journal of Geodesy and Geoinformation"

Martin Metzner

Member of the NA 005-03-01 AA "Geodäsie" at the DIN German Institute for Standardization

Course Director of the MSc Program GeoEngine at the University of Stuttgart

Li Zhang

Chair of the Working Group 5.6 "Cost Effective Positioning" within the FIG Commission 5 (Positioning and Measurement),

Chair of the Working Group "Quality Assurance" within the Commission 3 "Measurement Methods and Systems" of "Deutscher Verein für Vermessungswesen (DVW)"

Doctorates

Hassan, Aiham

Entwicklung eines tachymeter-basierten Zielsystems. Universität Stuttgart: Universitätsbibliothek der Universität Stuttgart

https://dx.doi.org/10.18419/opus-13878

Main reviewer: Prof. Dr.-Ing. habil. Dr. h.c. Volker Schwieger,
Co-reviewers: Prof. Dr.-Ing. Andreas Eichhorn (TU Darmstadt), Prof. Dr.-Ing. Ingo Neumann (Leibniz Universität Hannover)

Yang, Yihui

Towards improved targetless registration and deformation analysis of TLS point clouds using patch-based segmentation. Universität Stuttgart: Universitätsbibliothek der Universität Stuttgart
https://dx.doi.org/10.18419/opus-13796
Main reviewer: Prof. Dr.-Ing. habil. Dr. h.c. Volker Schwieger,
Co-reviewer: Prof. Dr. Corinna Harmening (KIT Karlsruhe), Prof. Dr.-Ing. Christoph Holst (TU München)

Kerekes, Gabriel

An elementary error model for terrestrial laser scanning. Deutsche Geodätische Kommission, Reihe C, Heft Nr. 900, ISBN 978 3 7696 5312-0, ISSN 0065-5325, Verlag der Bayerischen Akademie der Wissenschaften
https://dgk.badw.de/fileadmin/user_upload/Files/DGK/docs/c-900.pdf
Main reviewer: Prof. Dr.-Ing. habil. Dr. h.c. Volker Schwieger,
Co-reviewer: Prof. Dr.-Ing. Hans-Berndt Neuner (TU Wien), Prof. Dr. Corinna Harmening (KIT Karlsruhe)

Master Theses

Chao, Yu Huang

A Road Network Path Analysis: Application for Emergency Response Vehicle Routing. (Luz/Sebald)

Helfert, Carsten

Entwicklung und Erprobung einer Potentialanalyse für Waldflurneuordnungen in Baden-Württemberg am Beispiel des Ostalbkreises. (Metzner)

Bachelor Theses

Hettich, Anna

Frühzeitige Bestimmung des Landabzuges in einem Flurbereinigungsverfahren. (Stadler/ Metzner)

Schankula, Patrick

Durchführung einer geometrischen Qualitätskontrolle mittels Trimble RealWorks. (Balangé/Schwieger)

Stahl, Alicia

> „Quo vadis Flurneuordnung Baden-Württemberg? Welche Bodenordnungsprodukte werden in Zukunft nachgefragt?" gewinnen Sie mit Daten von gestern schon heute die Antworten auf die Fragen von Morgen. (Stadler/ Metzner)

Education

SS23 and WS23/24 with Lectures/Exercises/Practical Work/Seminars

Bachelor Geodesy and Geoinformatics (German)

Basic Geodetic Field Work (Frolow, Kanzler)	0/0/5 days/0
Engineering Geodesy I (Schwieger, Kerekes/Abolhasani)	4/2/0/0
Engineering Geodesy II (Schwieger, Gorokhova)	1/1/0/0
Geodetic Measurement Techniques I (Metzner, Frolow)	3/1/0/0
Geodetic Measurement Techniques II (Frolow)	0/1/0/0
Integrated Field Work (Miehling, Metzner)	0/0/10 days/0
Reorganisation of Rural Regions (Stadler)	1/0/0/0
Statistics and Error Theory (Schwieger, Balangé)	2/2/0/0

Master Geodesy and Geoinformatics (German)

Deformation Analysis (Zhang)	1/1/0/0
Industrial Metrology (Schwieger, Gorokhova)	1/1/0/0
Land Development (Eisenmann)	1/0/0/0
Monitoring Measurements (Schwieger, Kerekes)	2/2/0/0
Terrestrial Multisensor Systems (Zhang, Frolow)	1/1/0/0
Geomobility (Zhang, Luz)	2/2/0/0

Master GeoEngine (English)

Kinematic Measurement Systems (Schwieger, Abolhasani)	2/2/0/0
Monitoring (Schwieger, Shevchuk)	1/1/0/0
Thematic Cartography (Zhang, Miehling)	1/1/0/0
Transport Telematics (Metzner, Sebald)	2/1/0/0
Terrestrial Multisensor Systems (Zhang, Shevchuk)	2/1/0/0

Bachelor and Master Aerospace Engineering (German)

Statistics for Aerospace Engineers (Zhang, Abolhasani)	1/1/0/0

Master Aerospace Engineering (German)

Industrial Metrology (Schwieger, Gorokhova)	1/1/0/0
Transport Telematics (Zhang, Luz)	2/2/0/0

Bachelor Civil Engineering (German)

Geodesy in Civil Engineering (Metzner, Luz, Kanzler)   2/2/0/0

Master Civil Engineering (German)

Geoinformation Systems (Metzner, Sebald)   2/1/0/0
Transport Telematics (Zhang, Luz)   2/1/0/0

Bachelor Transport Engineering (German)

Seminar Introduction in Transport Engineering (Sebald)   0/0/0/1

Master Infrastructure Planning (English)

GIS-based Data Acquisition (Zhang, Kerekes)   1/1/0/0

Institute of Geodesy

Geschwister-Scholl-Str. 24D
70174 Stuttgart
+49 711 685 83390
gis@gis.uni-stuttgart.de
www.gis.uni-stuttgart.de

Institute Management

Prof. Dr.-Ing. Nico Sneeuw	Head, Chair of Geodesy
Prof. Dr. James Foster	Chair of Space Geodetic Methods
Dr.-Ing. Mohammad Tourian	Senior Scientist, Satellite Geodesy

Retired

Prof. Dr. sc. techn. Wolfgang Keller

Academic Staff

Dr.-Ing. Markus Antoni	Physical Geodesy, Satellite Geodesy (until February 2023)
M.Sc. Clara Beck	Physical Geodesy, Seismology
Dr. Yixiati Dilixiati	Physical Geodesy
Dr. Karim Douch	Physical Geodesy, Seismology (until June 2023)
Dr.-Ing. Omid Elmi	Remote Sensing
PD Dr.-Ing. habil. Johannes Engels	Physical Geodesy, Satellite Geodesy
M.Sc. Shahin Khalili	Satellite Altimetry (from December 2023)
Dr.-Ing. Peyman Saemian	Satellite Geodesy, Hydrology
M.Sc. Bruce Thomas	Physical Geodesy, Satellite Geodesy
Ph.D. Rudolf Widmer-Schnidrig	Physical Geodesy, Seismology

Research Associates

M.Sc. Sajedeh Behnia	Satellite Altimetry
M.Sc. Siqi Ke	Hydrology
M.Sc. Bo Wang	Satellite Altimetry
M.Sc. Shuhua Yu	Satellite Altimetry (from October 2023)

Administrative/Technical Staff

B.A. Tamara De Francesco	Secretary
Dipl.-Ing. (FH) Thomas Götz	IT, Controlling
Dipl.-Ing. (FH) Ron Schlesinger	IT, Technical Support, Gravimetry

External Lecturers

Dipl.-Ing. Gerhard Grams	Ministerium für Ländlichen Raum und Verbraucherschutz Baden-Württemberg, Stuttgart
Dipl.-Ing. Dieter Heß	Ministerium für Ländlichen Raum und Verbraucherschutz Baden-Württemberg, Stuttgart

Guests

Dr.-Ing. Xiaole Deng	Southern University of Science and Technology, Shenzhen, China, Humboldt Fellow
M.Sc. Albertini Nsiah Ababio	Hong Kong Polytechnic University, RSAP (since December 2023)
Prof. Dr.-Ing. Dimitrios Tsoulis	Aristotle University of Thessaloniki, Greece, Humboldt Fellow (June - August 2023)
Dr. Zhourun Ye	Hefei University of Technology, Hefei, China, CSC (since December 2023)

Research

The performance of SWOT nadir altimeter for monitoring inland water bodies: A first assessment

Surface Water and Ocean Topography (SWOT) is a satellite mission that commenced its operations in the planned science orbit in late July 2023, following its launch in December 2022. Before entering the science orbit, the satellite spent three months in a one-day repeat orbit for Calibration and Validation (Cal/Val) purposes. SWOT's primary sensor for the measurement of lakes and rivers is the Ka-band Radar Interferometer (KaRIN). However, due to the presence of a 20-km gap between the right and left swath, certain lakes and river reaches across the globe will remain unmonitored by SWOT KaRIN. SWOT's secondary sensor, the nadir altimeter Poseidon-3C, covers these otherwise unmonitored water bodies. Hence, it becomes important to assess the performance of SWOT nadir altimetry over inland water bodies. The Cal/Val orbit provides a unique opportunity for such an evaluation, as it provides daily water level time series data. Among the 1011 lakes and reservoirs worldwide underneath the Cal/Val orbit, we acquire meaningful daily time series for 193 of them (Figure 1), enabling a comprehensive assessment of the SWOT nadir's monitoring capabilities. Our results show that the Offset Centre of Gravity (OCOG) and the Threshold First Maxima Retracker (TFRMRA) outperform other retrackers (e.g. Figure 2). The decimeter-level accuracy offered raises optimism regarding the potential applicability of SWOT nadir observations to achieve a near-full coverage of water bodies on Earth.
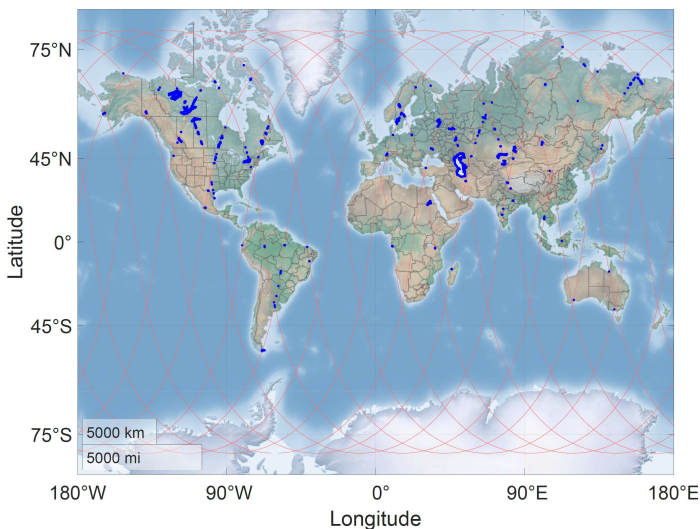

Figure 1: The ground track of SWOT's nadir altimeter, Poseidon-3C, is shown with 193 lakes highlighted in blue, from which meaningful daily water level time series are obtained.
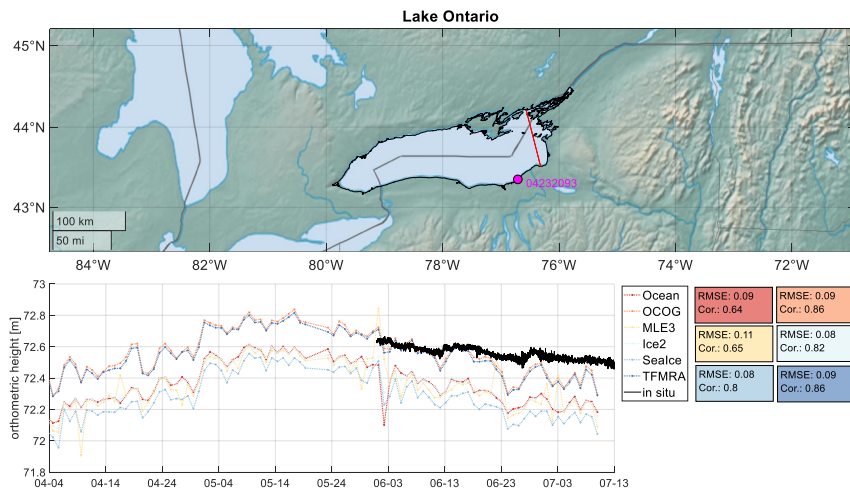
Figure 2: Results from the SWOT nadir altimeter during the Cal/Val phase over Lake Ontario, using various retrackers, are compared with in situ data measured at the USGS station 04232093 (magenta). The Threshold First Maxima Retracker (TFRMRA) and the Offset Centre of Gravity (OCOG) retrackers, displaying a correlation of 0.86, demonstrate better performance compared to other retrackers.

Fault tolerant approach to regenerate Level-1B SAR altimetry waveforms for enhancing Level-2 retrackers performance

This study deals with the identification and retrieval of anomalous waveforms generated in the Level 1B processing chain of satellite altimetry over coastal areas and inland water bodies. Efficient identification of anomalous waveforms greatly improves the retracking performance, leading to the generation of precise water level time series that serve as vital inputs for hydrological studies. Abnormal behaviour in waveforms may be an indication of environmental changes, instrument malfunctions, or other critical factors. To find anomalous waveforms, our framework utilizes an unsupervised machine-learning technique. We categorize different parameters of the satellite's altimeter like AGC parameter, tracker range, and features related to the shape of waveforms, for instance, waveform's skewness, number and location of peaks, and so on for each sample in the dataset. Then we identify abnormal waveforms using a two-step density distribution probability analysis.

For instance, after applying the method for anomalous waveform detection on Lake Boca as a case study of small lakes, measured by the Sentinel-3B Satellite, as demonstrated in figure 3 two waveforms in the dataset identified as abnormal.
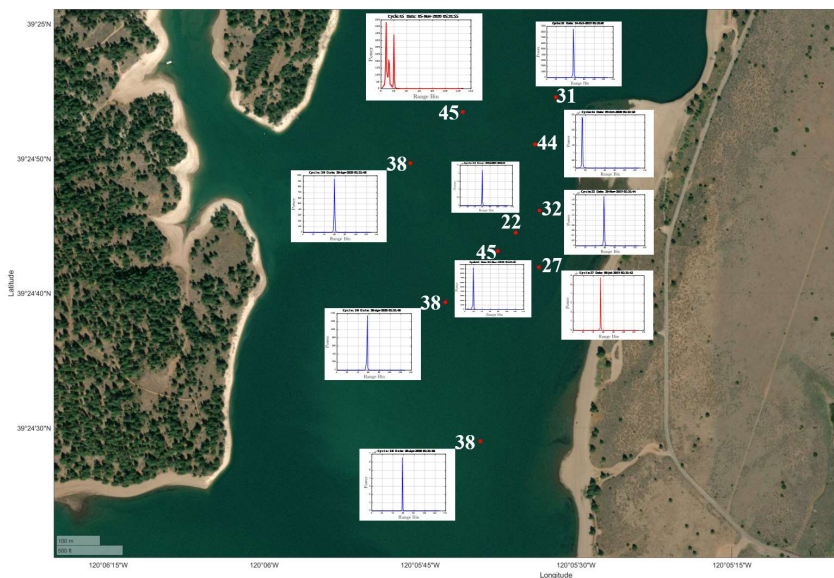
Figure 3: The plotted red waveforms represent abnormal, while the blue waveforms represent normal data in the dataset with their corresponding cycle number over Lake Boca.

The secondary purpose of this study is to propose a robust strategy to retrieve abnormal waveforms in the level 1B SAR processing chain. This step is vital for narrow rivers and small inland water bodies, in which a low number of measurements on related cycles cause missing hydrology data. In contrast to previous studies focusing solely on investigating L2 waveforms to determine precise retracking gates for multipeak and noisy waveforms, we propose an additional step in the L1B processing chain, specifically tailored to coastal and inland waters, enabling the retrieval of abnormal waveforms. In both fully focused and unfocused SAR processing, the final waveform is formed through the combination of various beam looks from the altimeter during fixed illumination time in stacks to the desired point on the surface, certain looks in the stack may exhibit undesirable patterns due to variations in environmental characterization, antenna footprint, and sidelobe gain. The proposed methods will mitigate the presence of undesirable waveforms in the stack prior to the generation of the final waveforms. Figure 4 gives an overview of the entire proposed strategy to detect and retrieve abnormal waveforms in the dataset.

We apply the proposed methodology for Sentinel 3A and 3B datasets over different inland waters and validated our results against in-situ data. The results demonstrate that the water level time series, obtained by regenerated waveforms have significantly improved. For instance, in the case of the Itaparica water reservoir, significant improvements are observed
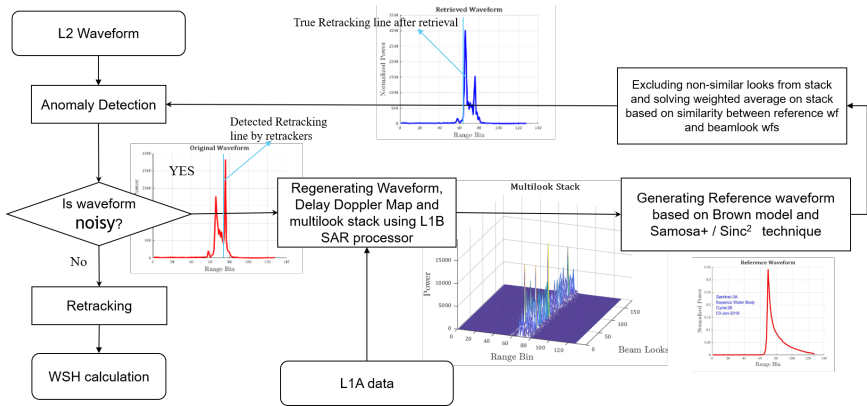
Figure 4: Overall procedure applied on waveforms of a dataset to regenerate clean waveforms.

after applying two different retracking methods, namely SAMOSA+ and OCOG, to both the original and enhanced waveforms, as demonstrated in the table 1.

Table 1: Evaluation of improvements achieved in performance of SAMOSA+ and OCOG Retrackers on enhanced waveforms generated by proposed method over Itaparica water reservoir

Case Study	Duration	L2 Retracker	Waveforms	RMSE (cm)	NSE	Correlation	Improvement in RMSE
Itaparica	2018-2019	SAMOSA+	Original Waveforms	7.7	0.89	0.98	40.25%
			Enhanced Waveforms	4.6	0.96	0.99	
		OCOG	Original Waveforms	11.8	0.74	0.97	61.01%
			Enhanced Waveforms	4.6	0.96	0.98	

The results show the potential of our proposed framework for detecting and retrieving anomalous waveforms leading to robust water level estimates from satellite altimetry data.

River surface slope determination from ICESat-2

ICESat-2 measures the topography along the ground track of 3 parallel pairs of laser beams spaced 3.3 km apart. This increases the probability of simultaneous water surface elevation measurements at different locations within a river reach. In this study, we will introduce a novel approach that capitalizes on the unique measurement geometry of ICESat-2 to obtain

instantaneous estimates of reach-scale river surface slope (RSS). This approach combines two methods, namely the across-track and along-track approaches. The along-track method involves fitting the RSS to all water surface elevations from each individual beam intersecting the river reach and projecting it onto the river's centerline. Additionally, the across-track method calculates the RSS by analyzing the simultaneous water surface elevations from ICESat-2's parallel beams that intersect a particular river reach. By combining these methods, a time-variable RSS is generated to maximize both temporal and spatial coverage. Moreover, an average reach-scale RSS is computed, aiming to derive the global average reach-scale RSS and its variability in future investigations.

In this study, we will estimate two types of RSS: (a) along-track-based river slope using a single beam, and (b) across-track river slope between two points on the centerline from two beams. We also use the estimated slopes to generate the slope time series and the averaged RSSs along the river. Figure **??** shows the schematic of ICESat-2 tracks intersecting the river extent. The river boundaries are represented by the blue curves, while the ground tracks of the 6 beams are depicted by the green lines. The red segments of the ground tracks indicate the areas where observations are made over the water surface. The centerline of the river is denoted by the blue dashed curve, and the orange points represent the intersections between the centerline and the ground tracks. Each red segment is characterized by an angle formed between the ground track and the centerline, which determines the slope of the segment, referred to as the along-track slope (i.e. the slope of each red segment). When the water level observations of the red segment are projected onto the centerline, it allows for the derivation of the along-track-based river slope. Each intersection (P_i) between the centerline and ground track has a water level value. By determining the distance between two intersections along the river's centerline, it becomes possible to estimate the across-track slope (e.g. the slope between P_1 and P_2). In the case depicted in Figure 5, it is observed that even a single beam, such as GT2L, can yield multiple intersections, as seen with the points of P_1 and P_2, while GT2R results in intersections P_3 and P_4.

We do not expect the slope between two gauge stations will reflect small-scale RSS, because the distance between two neighboring gauge stations is much larger than the length of a reach. However, when calculating the across-track slope using two strong beams, e.g. the slope between P_2 and P_5 in Figure 6, the two weak beams will also generate one across-track slope. As a result, the across-track slope can be compared between both strong and weak beams. The across-track slopes from strong beams within each reach over four years are averaged, providing a representative value for the across-track slope of that reach. This process is similarly applied to the weak beams, obtaining the chainage slopes for both strong and weak beams. Figure 6 shows the chainage slope of the river derived from strong and weak beams. The color bar indicates that the slopes of upstream reaches are steeper compared to those of downstream reaches. In Figure 6(b), there is a data gap between 49°N and 50°N, resulting from the lack of available data on weak beams in that region. Notably, the slope difference between strong and weak beams is relatively small in the downstream section, specifically from 49°N heading northwards, with a RMS of 3.2 cm/km. In the upstream section, specifically from 49°N heading southwards, the slope difference between strong and
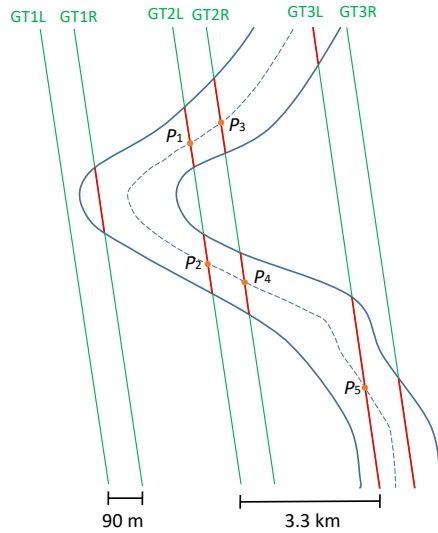
Figure 5: Schematic of ICESat-2 tracks intersecting the river extent.

weak beams is more significant compared to the downstream part, with a RMS of 9.7 cm/km. Several factors may contribute to this difference, including substantial slope variations, the presence of dams, and potential obstructions such as wires in the upstream region.
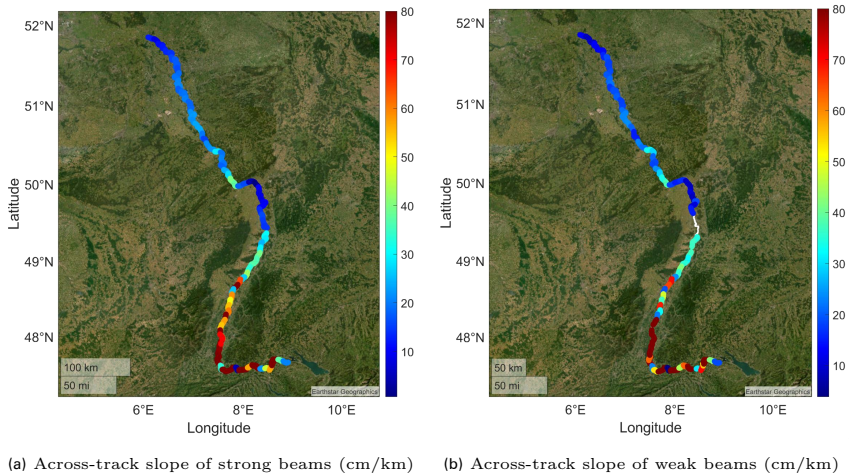

(a) Across-track slope of strong beams (cm/km)

(b) Across-track slope of weak beams (cm/km)

Figure 6: Comparison of across-track slopes between strong and weak beams.

Remote Sensing-Based Extension of GRDC Discharge Time Series - A Monthly Product with Uncertainty Estimates

The global river network, though covering less than 1% of the Earth's non-glacial surface and containing less than 0.01% of its freshwater, serves as a vital resource for human well-being and natural processes as one of the most accessible sources of freshwater. River discharge measurements from global river gauges are fundamental to hydrologic science and are considered as a baseline for water resource management. The Global Runoff Data Center (GRDC) collects and provides quality-controlled discharge observations worldwide, extensively utilized by the scientific community to explore the interactions among the water cycle, climate, and ecosystems. However, the GRDC dataset has experienced a decline in active gauges since the 1980s, with only 14% remaining active as of 2020. This decline leaves many river basins poorly gauged, ungauged, or lacking an open-data policy for their gauges. Therefore, our understanding of the amount of water flowing through the world's rivers is inaccurate, inhibiting a clear insight into the global spatial and temporal dynamics of river water.

To address the limitations in global discharge measurements, we introduce the Remote Sensing-based Extension for the GRDC (RSEG) dataset. This data set is designed to incorporate legacy gauge discharge data and remote sensing observations. Utilizing a stochastic nonparametric mapping algorithm, we extend the monthly discharge time series for inactive GRDC stations, leveraging satellite imagery and altimetry data on river width and water height (see Figure 7 - top panel). Afterward, a rigorous quality assessment of the estimated discharge results in the extension of discharge records for 3377 out of 6015 GRDC stations with a mean monthly discharge larger than $10\,\mathrm{m^3/s}$.

We conduct validation of the RSEG dataset against gauge discharge records. The accuracy of discharge estimates is notably high for rivers with a large or medium mean discharge (average KGE value > 0.5). However, for river reaches with a low mean discharge, the average KGE value decreases to 0.33, primarily due to the absence of high-quality remote sensing data for narrow river stretches. The RSEG dataset restores monitoring capability for 83% of the total river discharge measured by GRDC stations, amounting to $7895\,\mathrm{km^3/month}$. The RSEG dataset holds significant potential for various research purposes, including integration into hydrological models to reduce model uncertainty, utilization as prior data for SWOT discharge algorithms to enhance their performance, and application in climate change and environmental studies to analyze long-term discharge trends.
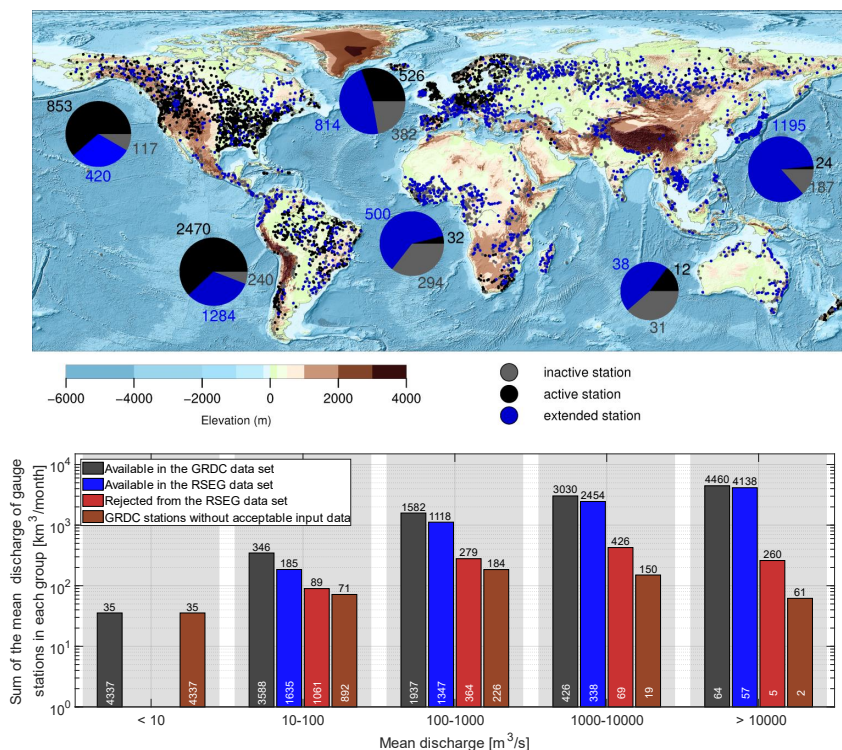
Figure 7: (top panel) location of the GRDC stations with a mean discharge larger than $10\,\mathrm{m^3/s}$. The GRDC stations that are active in 2015 are presented in black, the inactive stations are in grey. The stations with discharge records extended through remote sensing data are shown in blue. The pie charts' area illustrates the river discharge on a logarithmic scale measured by active (black), inactive (grey) and extended (blue) GRDC gauges by continent. The numbers indicate the accumulated discharge over stations in $\mathrm{km^3/month}$. (bottom panel) bar graphs showing discharge (in $\mathrm{km^3/month}$) accumulated over GRDC stations in five discharge classes. Note that in the first category, those stations with mean discharge smaller than $10\,\mathrm{m^3/s}$ are excluded. The blue bars depict discharge estimates available in the RSEG data sets, the red bars represent discharges that were rejected during the quality control steps, and the brown bars indicate cases without suitable remote sensing observations. The numbers on top of the bars indicate the discharge volume in $\mathrm{km^3/month}$, while the numbers on the bar feet represent the number of stations.

A Method for Estimating Daily Discharge Using Space-based Discharge Estimates

An accurate estimate of river discharge is vital to quantifying the global hydrological cycle and managing water resources. Given the steadily deteriorating data provision from gauge

networks, hydrological monitoring through spaceborne sensors becomes a necessity. The SWOT mission is the first satellite to conduct a global survey of the Earth's surface waters, measuring water surface elevation, river width, and surface slope for estimating discharge. Since SWOT can only sample mid-latitude locations approximately twice per its 21-day cycle, we develop a linear dynamic system for daily discharge estimation over continuous reaches in a single-branch river network. The linear dynamic system includes a process model based on a physically-based spatiotemporal correlation model and observation equations utilizing SWOT products. Figure 8 shows the concept of the dynamic system through a simple sketch. We solve this dynamic system through a Kalman filter, which is simultaneously executed in the time and space domains to obtain daily discharge. Since SWOT discharge products are currently inaccessible, we use the perturbed version of synthetic SWOT datasets, which contains 15 test cases, obtained by Monte Carlo simulations to test the feasibility of our approach.
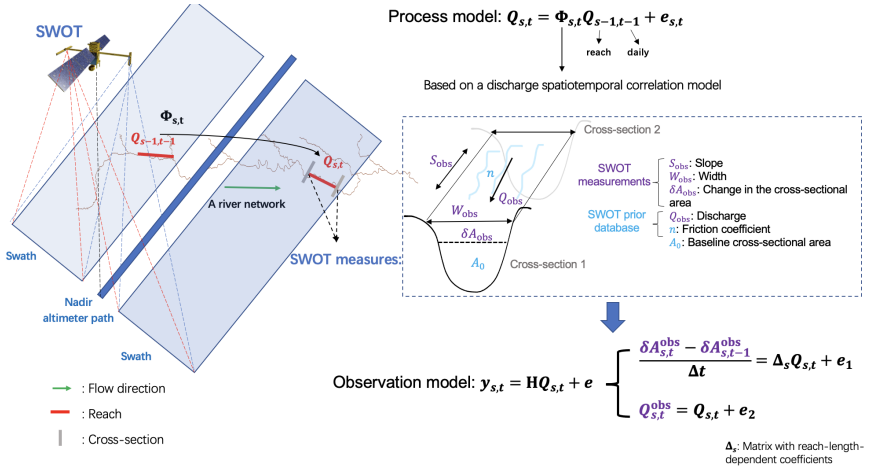

Figure 8: Concept of the dynamic system. In the sketch, there is a river network measured by SWOT. We can use the linear dynamic system to estimate the daily discharge of reaches for it. The linear dynamic system includes a process model based on a physically-based spatiotemporal correlation mdoel and observation equations utilizing SWOT products.

After Kalman filtering, we obtain the daily discharge in time series at each reach without data outages. Due to our special configuration of the state vector and prediction scheme, we obtain more than one estimate per day at each reach. Therefore, we built 25 (22 discharge sets extracted directly from realizations $Q_{\mathrm{est}(1\sim22)}^{\mathrm{ptb}}$, as well as the weighted mean $Q_{\mathrm{est(wm)}}^{\mathrm{ptb}}$, arithmetic mean $Q_{\mathrm{est(am)}}^{\mathrm{ptb}}$ and median discharge sets $Q_{\mathrm{est(med)}}^{\mathrm{ptb}}$) combination ensembles for the outcomes. For the purposes of evaluation of our dynamic system, we validated the estimated discharge against true discharge using the performance metrics correlation, NSE, RMSE, and relative bias. As crucial benchmarks, we also validated the observed discharge

as well as the linearly interpolated daily discharge using observed discharge against true discharge, respectively. Figure 9 shows the estimated daily river discharge for reaches in test case Ohio Section 2 one of the test cases, using perturbed datasets: $Q_{\text{est}(1\sim22)}^{\text{ptb}}$ (gray curves), $Q_{\text{est}(wm)}^{\text{ptb}}$ (yellow curves), $Q_{\text{est}(am)}^{\text{ptb}}$ (green curves), and $Q_{\text{est}(med)}^{\text{ptb}}$ (red curves), compared to the true discharge Q_{true} (black curves) and the observed discharge in SWOT sampling $Q_{\text{obs}}^{\text{ptb}}$ (blue asterisks). We can see that the behavior of our estimated discharge for all reaches generally reflects that of variation of the true discharge. Generally, the optimal median validation values over reaches among the 25 ensembles indicate a correlation of -0.18–0.95, NSE for residuals of -1.48–0.82, rRMSE for residuals of 45%–330%, and relative bias of 5%–485%, while the observed discharge shows a median correlation of 0.22–0.99, median NSE for residuals of -7.20–0.96, median rRMSE for residuals of 21%–286%, and median relative bias of 11%–506%, and the interpolated daily discharge is 0.16–0.97, -5.7–0.88, 35%–258%, and 11%–508%, respectively. By comparing estimated and observed discharge, we can conclude that our estimates are close to the observed discharge in terms of correlation, NSE, and rRMSE and usually outperform it in terms of relative bias and CDF plots of errors. It goes without saying that our estimated discharge outperforms the simple interpolation method.
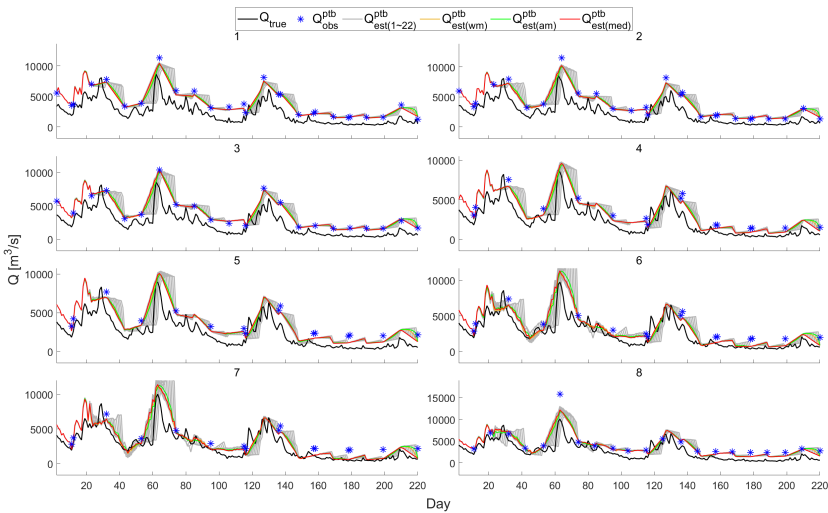

Figure 9: Estimated daily river discharge of reaches in Ohio Section 2, one of the test cases, using perturbed datasets, including $Q_{\text{est}(1\sim22)}^{\text{ptb}}$ ($1\sim22$: 1st to 22nd discharge set, gray curves), $Q_{\text{est}(wm)}^{\text{ptb}}$ (wm: weighted-mean discharge set, yellow curves), $Q_{\text{est}(am)}^{\text{ptb}}$ (am: arithmetic-mean discharge set, green curves), and $Q_{\text{est}(med)}^{\text{ptb}}$ (med: median discharge set, red curves), compared to the true discharge Q_{true} (black curves) and the SWOT-sampled discharge observations $Q_{\text{obs}}^{\text{ptb}}$ (blue asterisks) in time series.

The results show that our method can generally successfully estimate river discharge at a daily resolution for the 15 test cases and reveals great potential once the required SWOT discharge products are available. In particular, although observations are unavailable at bad reaches and significantly biased at many reaches, our estimates can nevertheless demonstrate considerably remarkable performance.

Global observation of an up to 9 day long, recurring, monochromatic seismic source near 10.9 mHz associated with tsunamigenic landslides in a Northeast Greenland fjord

This activity report summarizes work that was triggered by the observation of a very peculiar and unique seismic signal in September of last year. On a Sunday afternoon, while doing a quick, remote state-of-health check of the continuously operating sensors at BFO, Rudolf Widmer-Schnidrig was immediately intrigued and puzzled by a signal that showed up on all our five broad-band seismometers and both gravimeter (Figure 10). In a collaborative and in-
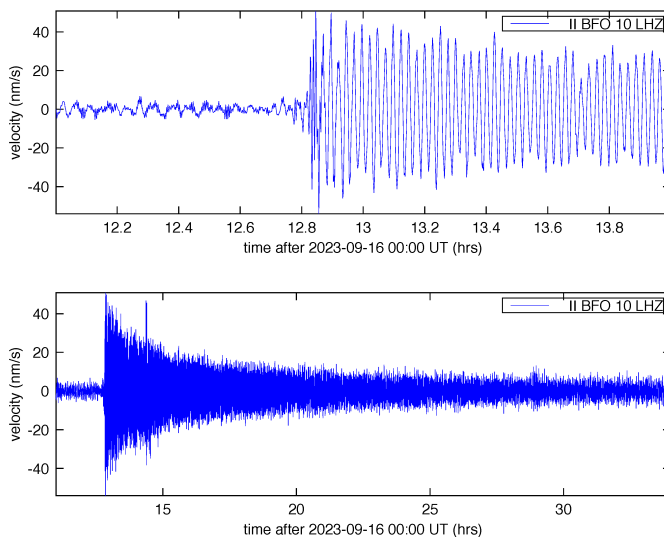

Figure 10: Two plots of the same seismogram band-pass filtered between 3-30 mHz. Top panel: close-up view of the onset of the signal. It is monochromatic right from the start with a frequency of 10.88 mHz and this monochromatic oscillation reaches its maximum amplitude after only approx. 3 cycles and decays monotonously from there on. Lower panel: the first day of data shows no amplitude modulation with time. The lack of any amplitude modulation is highly unusual and unlike the signal from large teleseismic events, where we typically see wave packets at 3-hour intervals.

terdisciplinary effort a team of over 80 international scientists, many of whom independently noticed the peculiar signal, got together and exchanged data, ideas, and analysis results over *mattermost*: an open source, web-based, online platform for collaborative research. This was a very novel way of doing research: together we got much further than we at BFO would have gotten on our own.

In our forthcoming EGU-2024 abstract we report the discovery of an unprecedented, monochromatic low-frequency seismic source arising from the fjords of North-East Greenland. Following a landslide and tsunami event in Dickson fjord on 16 September 2023, the seismic waves were detected by broad-band seismometers worldwide. Both frequency and phase velocity of the waves are consistent with fundamental mode Rayleigh- and Love-waves. However, the decay rate of these waves is much slower than predicted for freely propagating surface waves. Therefore, we infer a long-lasting and slowly decaying source process. Although the 16 September 2023 event was by far the largest, analysis of historical seismic data has revealed five other previously undetected events, all with a fundamental frequency between 10.85 and 11.02 mHz. Of these six events, the signal of the largest two events initially decayed with a quality factor, Q close to Q=500, which increased to Q=3000 within the first 10 hours and could thus be detected for up to nine days. The smaller four events had a slow decay-rate (Q>1000) for their entire duration. In comparison, the global average attenuation of Rayleigh waves at these frequencies is Q=117 for the PREM reference Earth model, thus precluding a single, impulsive source for these signals. Gleaning archives of optical and SAR satellite images reveal that four out of six events could be temporally correlated with landslides in Dickson fjord, the two others remain unresolved. However, such rapid transient events cannot explain the long duration of the radiated seismic waves. Our modeling of the largest event shows that a transversal seiche in Dickson fjord, excited by a landslide-induced tsunami, can account for both the monochromatic, low-frequency signal as well as its seismic signal amplitude and radiation pattern. However, the seiche modeling indicates that the seiche should have $Q < 250$. Therefore, it remains unclear what keeps the seiche going for the entire duration of the observed seismic signal. However, the phase coherence of the VLP signal (Fig. 11) leads some of us to conjecture that an as yet undetermined, in-phase, force feedback mechanism such as depicted in Fig 12 may be at work to continuously add energy into the system.

We plan to heavily instrument Dickson fjord in the summer of 2024 in the hope of shedding more light on the source mechanism of this still enigmatic, long-lasting, monochromatic, seismic signal.
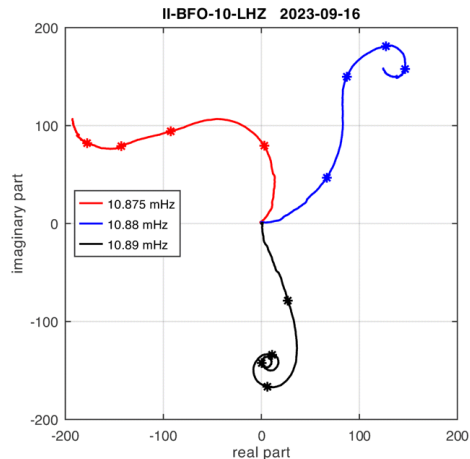
Figure 11: Phasor walks for the initial 50 hours of the VLP signal recorded by the STS-6A seismometer at BFO (see Figure 10). A phasor walk is a graphic representation of how the complex Fourier coefficient at a particular frequency grows with the length of the time series. The three phasor walks start at the origin of the complex plane and are marked with an asterisk in 10-hour intervals. The frequencies for the three walks was chosen to cover the band covered by the VLP signal. All three walks are initially curved counterclockwise before they curl in the clockwise direction. This slow change in curvature is indicative of a slow change in the VLP frequency. The angle under which a phasor-walk departs from the origin is arbitrary: by changing the start time by only a fraction of the signal period (92s) any take-off angle can be obtained. The shape of the phasor-walk, however, remains unchanged. The lack of any sudden changes in direction argues against a model in which the seiche gets sustained by discrete impulsive events, such as additional rock avalanches into the fjord or wind gusts.
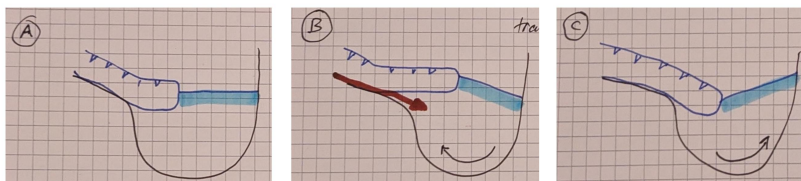
Figure 12: Cartoon for a conceptual model that goes a long way to explain the observed monochromatic seismic signal. The panels show three snapshots of a transversal seiche in a fjord. The long axis of the fjord is in the figure plane. From the left, a glacier enters the fjord. (A) The water is at rest and a glacier tongue floats on the fjord. (B) A transversal seiche is excited. The glacier tongue gets uplifted by the seiche and thereby opens a conduit for a stream on pressurized, subglacial water entering the fjord in the form of a jet. The water jet (red) pushes the water in the fjord back and reexcites the seiche. (C) Half a seiche cycle later the glacier tongue has moved down and the subglacial conduit is blocked by the glacier tongue. Taken together this is a frequency-selective mechanism to drive a transversal seiche as long as there is enough water draining into the fjord. The principal problem with this model is certainly that we have so far not been able to identify the glacier that should be involved in this process.

Evaluation of gravitational curvatures for a tesseroid and spherical shell with arbitrary order polynomial density

In recent years, there are research trends from constant to variable density and low-order to high-order gravitational potential gradients in gravity field modeling. Under the research circumstances, we focus on the variable density model for gravitational curvatures (or gravity curvatures, third-order derivatives of gravitational potential) of a tesseroid (see Fig. 13) and spherical shell in the spatial domain of gravity field modeling.
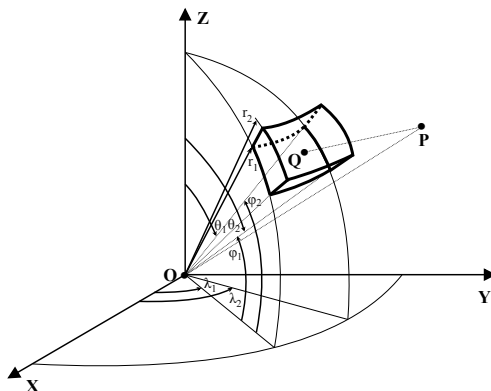

Figure 13: Illustration of a tesseroid in the spherical coordinate system

In this contribution, the general formula of the gravitational curvatures of a tesseroid with arbitrary order polynomial density is derived. The general expressions for gravitational effects up to the gravitational curvatures of a spherical shell with arbitrary order polynomial density are derived when the computation point is located above, inside, and below the spherical shell. When the computation point is located above the spherical shell, the general expressions for the mass of a spherical shell and the relation between the radial gravitational effects up to arbitrary order and the mass of a spherical shell with arbitrary order polynomial density are derived. The influence of the computation point's height and latitude on gravitational curvatures with the polynomial density up to fourth order is numerically investigated using tesseroids to discretize a spherical shell. Numerical results reveal that the near-zone problem exists for the fourth-order polynomial density of the gravitational curvatures, i.e., relative errors in $\log_{10}$ scale of gravitational curvatures are large than 0 below the height of about 50 km by a grid size of $15' \times 15'$. The polar-singularity problem does not occur for the gravitational curvatures with polynomial density up to fourth order because of the Cartesian integral kernels of the tesseroid. The density variation can be revealed in the absolute errors as the superposition effects of Laplace parameters of gravitational curvatures other than the relative errors. The derived expressions are examples of the high-order gravitational potential gradients of the mass body with variable density in the spatial domain, which will

provide the theoretical basis for future applications of gravity field modeling in geodesy and geophysics.

Analytical Solutions for Gravitational Potential up to its Third-order Derivatives of a Tesseroid, Spherical Zonal Band and Spherical Shell

The spherical shell and spherical zonal band are two elemental geometries that are often used as benchmarks for gravity field modeling. When applying the spherical shell and spherical zonal band discretized into tesseroids, the errors may be reduced or cancelled for the superposition of the tesseroids due to the spherical symmetry of the spherical shell and spherical zonal band (see Fig. 14).
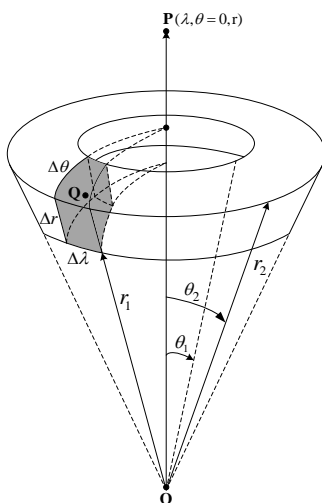

Figure 14: Visualization of a tesseroid (i.e., shadow part) and a spherical zonal band

In previous studies, this superposition error elimination effect (SEEE) of the spherical shell and spherical zonal band has not been taken seriously, and it needs to be investigated carefully. In this contribution, the analytical formulas of the signal of derivatives of the gravitational potential up to third-order (e.g., V, V_z, V_{zz}, V_{xx}, V_{yy}, V_{zzz}, V_{xxz}, and V_{yyz}) of a tesseroid are derived when the computation point is situated on the polar axis. In comparison to prior research, simpler analytical expressions of the gravitational effects of a spherical zonal band are derived from these novel expressions of a tesseroid. In the numerical experiments, the relative errors of the gravitational effects of the individual tesseroid are compared to those of the spherical zonal band and spherical shell not only with different 3D Gauss-Legendre quadrature orders ranging from (1,1,1) to (7,7,7) but also with different grid sizes (i.e., $5° \times 5°$, $2° \times 2°$, $1° \times 1°$, $30' \times 30'$, and $15' \times 15'$) at a satellite altitude of 260

km. Numerical results reveal that the SEEE does not occur for the gravitational components V, V_z, V_{zz}, and V_{zzz} of a spherical zonal band discretized into tesseroids. The SEEE can be found for the V_{xx} and V_{yy} whereas the superposition error effect exists for the V_{xxz} and V_{yyz} of a spherical zonal band discretized into tesseroids on the overall average. In most instances, the SEEE occurs for a spherical shell discretized into tesseroids. In summary, numerical experiments demonstrate the existence of the SEEE of a spherical zonal band and a spherical shell, and the analytical solutions for a tesseroid can benefit the investigation of the SEEE. The single tesseroid benchmark can be proposed in comparison to the spherical shell and spherical zonal band benchmarks in gravity field modeling based on these new analytical formulas of a tesseroid.

Forward modeling of a tesseroid in spectral domain

Gravity forward modeling is an important topic for geodesy and geophysics. It is also the prerequisite for inversion which seeks to estimate the mass distribution from gravity observation. In practice, the targeted mass distribution is discretized into regular shaped mass bodies (e.g. point mass, cylinder, prism and tesseroid) and can be computed through analytical or numerical integration. Tesseroids are suitable for large-scale or global-scale modeling when we take into account the sphericity of the Earth. Gravity forward modeling using tesseroids is usually carried out in the spatial domain. For the special case, there is an analytical solution for the gravitational potential of a tesseroid evaluated at the polar axis. For more general cases, the gravity functionals are calculated through numerical integration. The focus of recent researches is to improve the accuracy and efficiency of the algorithm. Nevertheless, these algorithms are implemented in the spatial domain so that the direct outputs are the gravity functionals which are calculated at a point or a grid in space. In contrast, we developed a new method to evaluate a tesseroid's effect in the spectral domain. We start from the same integral form of Newton's law of gravitation and combine it with the spherical harmonic addition theorem. As a result, the gravitational potential of a tesseroid can be directly given in spherical harmonic coefficients. In addition, we expanded the spherical harmonic coefficients at polar axis where the analytical expression of gravitational potential also exists for a tesseroid. We compared the result of our method with this ground truth. A $1° \times 1°$ single tesseroid is placed in mid-latitude (45°N,45°E), whose lower bottom is 20 km beneath the surface and the top is 10 km below the surface. The relative error shows a periodicity in the log scale. The new spectral method is not superior in terms of speed or precision. However, it could be useful for a specific user case (e.g. for a band-limited signal) because a tesseoid's effect can be evaluated in any spectral bandwidth.

NGGM/MAGIC simulation for mantle gravity signals

GRACE and GRACE-FO missions have been successfully providing the time-variable gravity field. The time-variable gravity field reflects the mass transportation in different spheres. It can be used to monitor the water circulation over the local and global scale (e.g., sea level rise, groundwater depletion, and glacial melting). It includes the signals that indicate the sub-
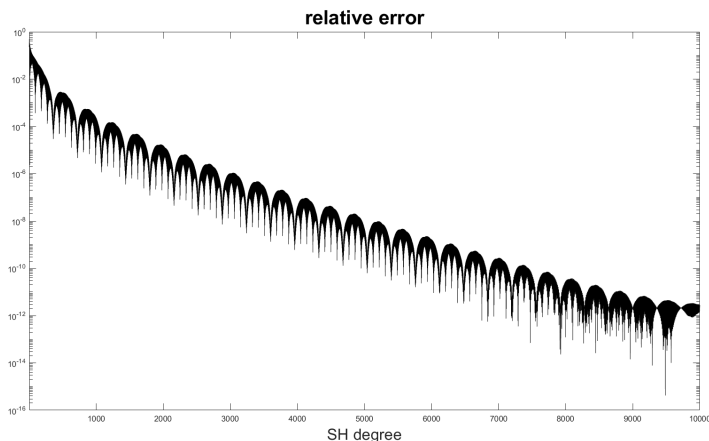
Figure 15: Relative error between spectral method and analytical solution

surface processes (e.g., glacial isostatic adjustment, and earthquakes). Overall, it provides valuable insights into Earth's dynamic processes. Numerous research topics have revealed successful findings including mass balance of major ice sheets, sea level rise, groundwater depletion, and co- and post-seismic gravity changes associated with an earthquake. However, these research findings are mainly related to the surface or shallow parts of the earth. There is no doubt that mass redistribution also occurs in the deeper interior of the earth, e.g., in the mantle. Mass transports in the mantle may affect the time-variable gravity field at decadal time scales. On the other hand, gravity field signals coming from mantle convection can give insight into the mantle viscosity which is a critical parameter for the geodynamic process of the earth's interior. Therefore, we are concerned with the challenges of the detectability of the gravity field stemming from the mantle convection. To this end, we carry out closed-loop simulation together with geodynamic modeling. The closed-loop simulation is carried out in a synthetic simulation environment where the true gravity model is already known. The true gravity model consists of a static gravity field (GOCO06s) and a time-variable gravity field (ESA Earth System Model). The synthetic observables are contaminated by a noise series related to the on-board instruments which is frequency dependent. A geodynamic model mimics the mantle-related gravity signal in a range of 50 years. We here show preliminary results on the detectability of mantle signals using a simulation setup together with simple white noise assigned to the instruments. We conducted a closed-loop simulation to identify mantle-related gravity signals generated by a geodynamic model, comparing our results with the monthly gravity solutions from GFZ. Ideally, the 10-year mantle-related gravity signal is detectable up to Spherical Harmonic (SH) degree 13 in a GRACE-like configuration and can be extended to SH degree 25 with a double pair satellite configuration. Advances in high-precision instruments now enable the detection of even a one-year mantle-

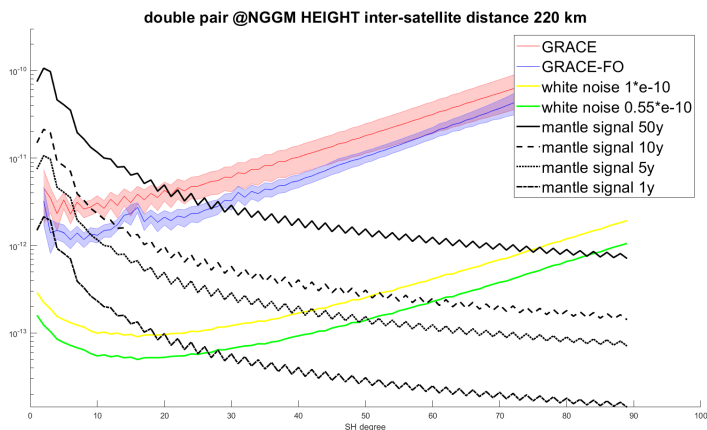related gravity signal up to SH degree 25, providing knowledge of the other time-variable gravity components.

Figure 16: Closed-loop simulation with white noise

Understanding Terrestrial Water Storage Variability and Trends: A Comprehensive Analysis

Terrestrial water storage (TWS), comprising groundwater, surface water, and ice, is integral for sustaining ecosystems and human activities. Understanding TWS dynamics is crucial for effective water resource management and climate change adaptation. Our comprehensive analysis, utilizing data from the Gravity Recovery and Climate Experiment (GRACE) missions, explores TWS variations across diverse sub-continental regions. Globally, TWS shows significant fluctuations. Negative trends in North America, Central Asia, and the Middle East challenge sustainable water resource management, while positive trends in Africa and the Amazon region add complexity. Addressing these challenges, we employed an ensemble of datasets for precipitation, evapotranspiration, and runoff, providing a holistic view of the water balance. Our study areas, covering 16 sub-continental regions, were carefully chosen to capture diverse hydrological conditions. Integration of surface water extent from the Hy-droSat dataset and satellite altimetric water level data enhances our understanding of TWS variations.

The sub-continental analysis revealed nuanced patterns of TWS changes Figure 17. Notably, North America witnessed a substantial TWS loss, amounting to approximately $2302\pm321\,\mathrm{km^3}$, driven by persistent negative trends that manifested since 2006. In contrast, Africa showcased a net TWS gain, accumulating an impressive $2380\pm165\,\mathrm{km^3}$. However, Central Asia and the Middle East grappled with pronounced losses, with Central Asia expe-

riencing a TWS decline of $590\pm99\,\mathrm{km}^3$ and the Middle East confronting a substantial loss of $813\pm70\,\mathrm{km}^3$. Flux balance analyses played a pivotal role in unraveling the intricate interplay of precipitation, evapotranspiration, and runoff on TWS dynamics. The influence of these factors was particularly pronounced in regions with notable TWS changes. For instance, the Indian sub-continent exhibited a significant TWS loss of $-527\pm29\,\mathrm{km}^3$, primarily attributed to the combined effects of precipitation, evapotranspiration, and runoff.

Surface water (SW) significantly influences TWS dynamics. The correlation analysis between TWS anomaly (TWSA) and SW indicates strong agreements (correlation coefficients, $r > 0.7$) in key regions: Australia ($r = 0.9$), Central Asia ($r = 0.86$), and East Africa ($r = 0.85$). Conversely, negative correlations are observed in regions like the Indian sub-continent, North Europe, West Europe, North America, and North Africa, where surface water plays a minimal role in TWS variations. For instance, North Europe and North America are predominantly influenced by snow and glacier melting, while groundwater extraction drives TWS changes in the Indian sub-continent. North Africa's TWS primarily reflects Sahara Desert variations, with surface water as low as $16\,\mathrm{km}^2$. West Europe demonstrates minimal surface water variations (<1 % of total) within the study period. Notably, fluctuations in surface water from lakes and reservoirs represent only a portion of the total surface water variations, as river systems, especially in regions like the Amazon (South America) and the Nile (Africa), contribute significantly to overall dynamics.
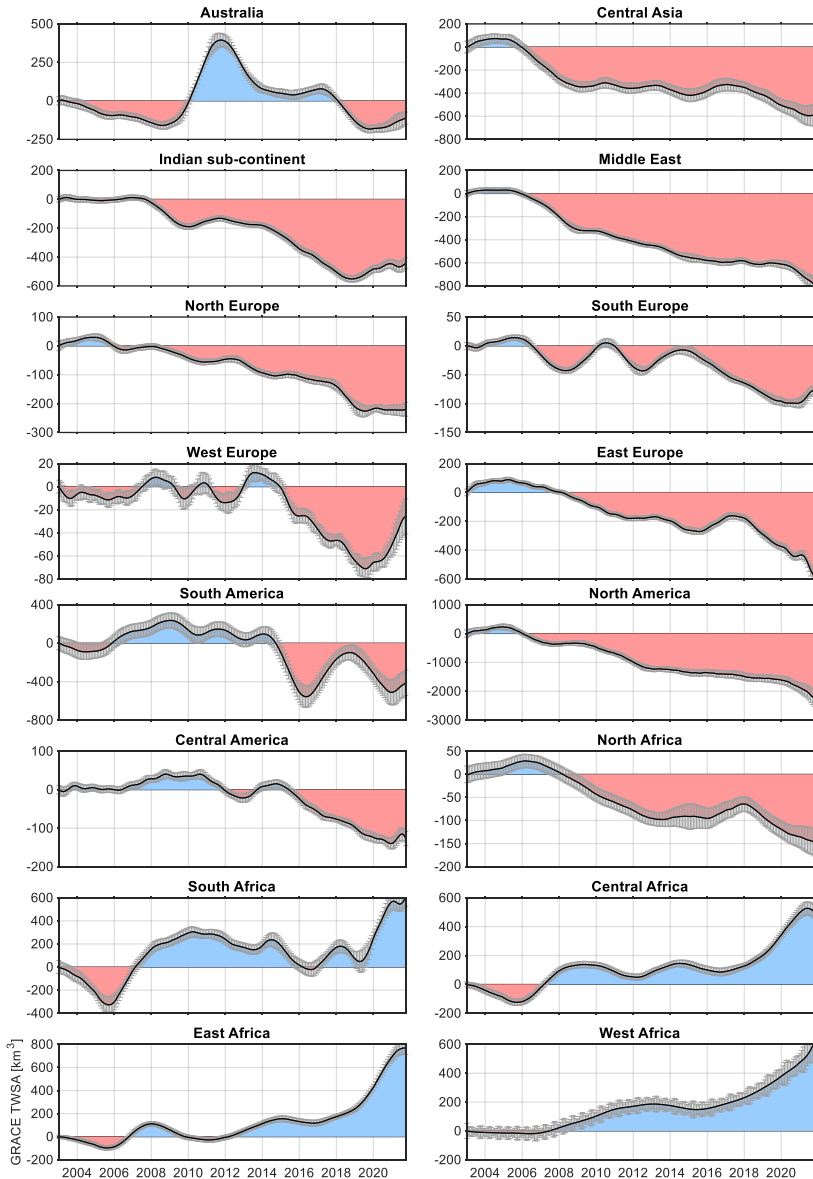
Figure 17: Inter-annual trend of TWSA estimated from Monte-Carlo Singular Spectrum analysis (MC-SSA) using the GRACE and GRACE-FO observations from 2003 to 2021 over subcontinents. The gain period is shown by the blue color and the loss period by red. The standard deviation of the trend estimation is shown with gray error bars, representing the uncertainty of the trend.

Seafloor Geodesy

Most of the world's largest earthquakes and tsunamis are formed on the decollement faults underlying subduction zones. Understanding the evolution and future behaviour of these fault systems requires an understanding of how seismic and aseismic slip processes interact on the fault. The relationships between the processes of interseismic creep, slow slip events, coseismic and postseismic slip define how stress is transferred and accumulated within the structure. Measurements from land-based geodetic sensors typically have a poor sensitivity geometry and to signals from the portion of the fault that approaches the seafloor. Seafloor geodetic techniques provide a way to make observations over this critically important zone. In particular GNSS-Acoustic techniques bring together standard GNSS positioning for a surface vehicle and acoustic ranging to link to seafloor sensors and determine their positions in the global reference frame. Performed by traditional research ships, this technique is very expensive to undertake, but the development of suitably equipped of unmanned surface vehicles - called Wave Gliders - has hugely reduced the cost of collecting GNSS-A data. A collaborative experiment between University of Stuttgart, and researchers at the U.S. Geological Survey, Scripps Institution of Oceanography, Lamont Doherty Earth Observatory, University of Washington, and University of North Carolina Wilmington, have been using a wave glider to make measurements over a portion of the Alaskan subduction zone. A great M8.2 earthquake in July 2021 occurred near one of our sites and we deployed our wave glider to measure the deformation produced by this event. We found nearly 1.5m of displacement - far greater than was detected by land-based GNSS sites, or predicted by the seismic data. We interpreted our results as showing that stresses in shallow portion of the fault zone, created by the coseimic slip on the deeper section of the fault were accommodated by post-seismic motion. As a consequence, rather than having increased, the risk of a major tsunamigenic event from this section of the fault had not changed.

A crucial problem for the GNSS-Acoustic technique is that the sound speed in the ocean is very variable, with a much greater magnitude perturbations than the analogous problem with atmospheric refraction for GNSS positioning. Characterizing and mitigating this noise source is the biggest current challenge for seafloor geodesy. In Alaska, we investigated this by examining a high-resolution numerical ocean model. Our GNSS-Acoustic survey strategy minimizes the impact of any vertical sound speed changes, but is susceptible to any lateral gradients in sound speed. We found that, for the site affected by the earthquake above, and one of the two others, the impact of sound speed gradients is likely small, with less than 1 cm of offset to the site position solutions 95% of the time. For the third site however, large local gradients exist most of the time, leading to offsets of nearly 2 cm half the time. While not significant in the case of large seismic motions above, this sort of error represents a big problem for the investigation of interseismic creep rates. These rates are what we use to estimate the likely magnitudes and recurrence rates for earthquakes at subduction zones, and was the motivation of the original Alaska seafloor geodesy experiment. This analysis, presented as an invited talk at the IUGG 2013 conference in Berlin, highlights the importance of a comprehensive investigation of sound speed variations in order to achieve the sub-cm positioning accuracies we are targeting for seafloor geodesy.
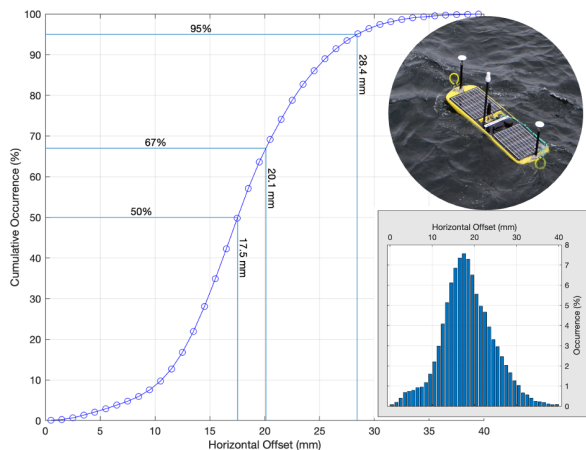
Figure 18: Cumulative occurrence of horizontal positioning offsets due to lateral sound speed gradients for Alaska GNSS-Acoustic site IVB1, based on the GOFS 3.1 high-resolution numerical ocean model. Inset Top: GNSS-Acoustic equipped wave glider; Inset Bottom: Histogram of horizontal offsets

Ability of a cargo-ship GNSS network to detect tsunamis

Tsunamis have claimed the lives of hundreds of thousands of people and are always associated with significant economic losses through infrastructure damages and costly evacuations. More temporal and spatial observations across the oceans are necessary to improve warnings and protect coastal communities. Recent studies demonstrate that a ship-based GNSS network analyzing in real-time the SSH is capable of detecting tsunamis even small amplitude tsunamis ($\sim 10\,\mathrm{cm}$), thus adding precise tsunami observations in an actual geodetic observational gap, and hence improving tsunami warning at a reasonable cost. We find that the commercial shipping fleet represents a vast existing infrastructure, with $\sim$38,000 ships in average at any time in the Pacific Ocean, with the ship density highest along coastlines and most source regions of tsunamis. One year of AIS records is studied and demonstrates that 73% of the Pacific Ocean is constantly covered by ships less than 1,000 km distant from each other, and more than 90% of the tsunami source regions are covered by a dense ship network that could augment local and regional early warning of near-field tsunamis (Figure 19). For far-field events, ships would be new observation points, improving in real-time models and enabling more effective and reliable tsunami forecasting and warning. For geographic regions less visited by large ships, several options are available to densify a potential observing ship network in these low-density coverage zones. Using the global cargo ship fleet, with its persistent spatial and temporal coverage, including in tsunamigenic regions, to form a ship-based GNSS network would be a cost-effective approach for augmenting tsunami detection. We would also like to acknowledge the contribution during this project

of Tasnîme Louartani from the ENSG-Geomatics school in France. A first paper on this topic has been submitted and under review at *The International Hydrographic Review*.
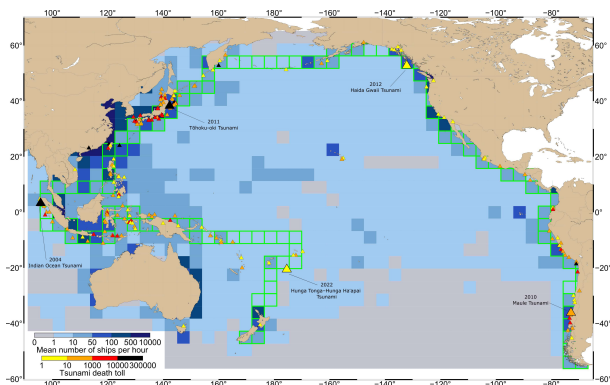

Figure 19: Map of the hourly mean number of ships per 500 km square, based on one year of AIS data provided by SPIRE Maritime. Triangles: source location of historic fatal tsunamis color-coded by death toll. Green highlighted cells locate the Pacific Ring of Fire, based on trench locations.

20 years of ground deformation patterns along Koa'e fault zone on Kīlauea volcano

Extreme long-term extensions are experienced along the Koa'e fault zone, a structural link between the East Rift zone and the Southwest Rift Zone on Kīlauea volcano. Both tectonic motions of the south flank of the volcano, as well as magma storage and transport at the summit and along the rift zones create stresses and ground motion patterns across this fault zone. To assess the role of Koa'e structure in these processes, and its contribution to hazard potential, this study investigates 20 years of survey GNSS data along a benchmark line running from south of Kīlauea's caldera through the Koa'e fault zone. This survey was realized by Bruce Thomas with the help of James Foster and Jon Avery (University of Hawai'i) in 2017, late 2021, late 2022 and early 2023 (Figure 20). We would also like to acknowledge the contribution during this project of Andi Ellis and David Phillips from the Hawaiian Volcano Observatory, as well as the help given by the Hawai'i Volcanoes National Park.

Advance in the Tsunami Early Warning Program in Hawai'i

Earthquake and Tsunami Early Warning (E/TEW) systems aim to provide a few crucial tens of seconds warning of imminent shaking. This allows people to move to safer locations, utilities to shut off gas and generators, and emergency response teams to prepare. However, the existing observing capacity for these traditional EEW ask for important financial resources

Figure 20: Fieldwork in progress on Kīlauea volcano.

for equipment and maintenance that not all countries can obtain. We propose a low-cost fixed network of smartphones, using the accelerometer and GPS chip embedded in and sensitive enough, to provide robust EEW and test TEW in the Hawaiian Islands. The approach follows the successful ASTUTI project in Costa Rica, by testing compact low-cost sensors to create a pilot network for low-cost E/TEW for the Big Island in Hawai'I (BiGi network). The sensors are smartphones and use the cell network to notify our server at the University of Hawai'i at Mānoa of any large earthquakes happening. The data from the accelerometer and the GNSS are used to produce (i) source models for earthquakes to estimate ground shaking, and (ii) slip models for large magnitude offshore earthquakes to assess seafloor deformation and model tsunami hazard. The project aims to demonstrate the capability of this type of low-cost network to rapidly detect large earthquakes and potential tsunami threats in Hawai'i. The sensors chosen are 4 Samsung J3 smartphones and 1 Xiaomi 8 smartphone, for its dual frequency GNSS chips enabling us to initiate numerical tsunami prediction models. The cell network is provided through a AT&T hotspot located near the smartphone. For the first test period, the smartphones were configured and deployed in locations close to previous earthquake swarms and in closed buildings around the island (Figure 21). We would also like to acknowledge the contribution of this project of Jon Avery, Chris Duncan, Todd Ericksen, and Ben Brooks.

Smartphone	Location
Xiaomi	Official building of Hawai'i Volcanoes National Park, close to the main Halema'uma'u crater of Kilauea.
Samsung 1	Official building of Hawai'i Volcanoes National Park, close to the main Halema'uma'u crater of Kilauea.
Samsung 2	Private house in Puna, on the south-east slop of Kilauea where the last 2018 eruption took place.
Samsung 3	Office at University of Hilo.
Samsung 4	Private house in Waimea (north of Kawaihae).

Figure 21: Location of the current 5 fixed smartphones for the BiGi network.

Publications

(https://www.gis.uni-stuttgart.de/en/research/publications/index.html)

Refereed Journal Publications

Brooks, B. A., D. Goldberg, J. DeSanto, T. L. Ericksen, S. C. Webb, S. L. Nooner, C. D. Chadwell, J. Foster, S. Minson, R. Witter, P. Haeussler, J. Freymueller, W. Barnhart, and J. Nevitt (2023): Rapid shallow megathrust afterslip from the 2021 M8.2 Chignik, Alaska earthquake revealed by seafloor geodesy. In: *Science Advances* 9.17, eadf9299. DOI: 10.1126/sciadv.adf9299.

Da Silva, E., E. R. Woolliams, N. Picot, J.-C. Poisson, H. Skourup, G. Moholdt, S. Fleury, S. Behnia, V. Favier, L. Arnaud, J. Aublanc, V. Fouqueau, N. Taburet, J. Renou, H. Yesou, A. Tarpanelli, S. Camici, R. M. Fredensborg Hansen, K. Nielsen, F. Vivier, F. Boy, R. Fjørtoft, M. Cancet, R. Ferrari, G. Picard, M. J. Tourian, N. Sneeuw, E. Munesa, M. Calzas, A. Paris, E. Le Meur, A. Rabatel, G. Valladeau, P. Bonnefond, S. Labroue, O. Andersen, M. El Hajj, F. Catapano, and P. Féménias (2023): Towards Operational Fiducial Reference Measurement (FRM) Data for the Calibration and Validation of the Sentinel-3 Surface Topography Mission over Inland Waters, Sea Ice, and Land Ice. In: *Remote Sensing* 15.19. DOI: 10.3390/rs15194826.

Deng, X. (2023a): Corrections to: "Accurate computation of gravitational field of a tesseroid" by Fukushima (2018) in J. Geod. 92(12):1371–1386. In: *Journal of Geodesy* 97.1, p. 8. DOI: 10.1007/s00190-022-01673-2.

Deng, X. (2023b): Evaluation of gravitational curvatures for a tesseroid and spherical shell with arbitrary-order polynomial density. In: *Journal of Geodesy* 97.2. DOI: 10.1007/s00190-023-01708-2.

Deng, X. and N. Sneeuw (2023a): Analytical Solutions for Gravitational Potential up to Its Third-order Derivatives of a Tesseroid, Spherical Zonal Band, and Spherical Shell. In: *Surveys in Geophysics*. DOI: 10.1007/s10712-023-09774-z.

Durand, M., C. J. Gleason, T. M. Pavelsky, R. de Prata Moraes Frasson, M. Turmon, C. H. David, E. H. Altenau, N. Tebaldi, K. Larnier, J. Monnier, P. O. Malaterre, H. Oubanas, G. H. Allen, B. Astifan, C. Brinkerhoff, P. D. Bates, D. Bjerklie, S. Coss, R. Dudley, L. Fenoglio, P.-A. Garambois, A. Getirana, P. Lin, S. A. Margulis, P. Matte, J. T. Minear, A. Muhebwa, M. Pan, D. Peters, R. Riggs, M. S. Sikder, T. Simmons, C. Stuurman, J. Taneja, A. Tarpanelli, K. Schulze, M. J. Tourian, and J. Wang (2023): A framework for estimating global river discharge from the Surface Water and Ocean Topography satellite mission. In: *Water Resources Research*, e2021WR031614. DOI: 10.1029/2021WR031614.

Elmi, O. and M. J. Tourian (2023): Retrieving time series of river water extent from global inland water data sets. In: *Journal of Hydrology* 617, p. 128880. DOI: 10.1016/j.jhydrol.2022.128880.

Kitambo, B. M., F. Papa, A. Paris, R. M. Tshimanga, F. Frappart, S. Calmant, O. Elmi, A. S. Fleischmann, M. Becker, M. J. Tourian, R. A. Jucá Oliveira, and S. Wongchuig (2023): A long-term monthly surface water storage dataset for the Congo basin from 1992 to 2015. In: *Earth System Science Data* 15.7, pp. 2957–2982. DOI: 10.5194/essd-15-2957-2023.

Onodera, K., K. Nishida, T. Kawamura, N. Murdoch, M. Drilleau, R. Otsuka, R. Lorenz, A. Horleston, R. Widmer-Schnidrig, M. Schimmel, S. Rodriguez, S. Carrasco, S. Tanaka, C. Perrin, P. Lognonné, A. Spiga, D. Banfield, M. Panning, and W. B. Banerdt (2023): Description of Martian Convective Vortices Observed by InSight and Implications for Vertical Vortex Structure and Subsurface Physical Properties. In: *Journal of Geophysical Research: Planets* 128.8, e2023JE007896. DOI: 10.1029/2023JE007896.

Pirooznia, M., M. Raoofian Naeeni, and M. J. Tourian (2023): Modeling total surface current in the Persian Gulf and the Oman Sea by combination of geodetic and hydrographic observations and assimilation with in situ current meter data. In: *Acta Geophysica* 71.6, pp. 2839–2863. DOI: 10.1007/s11600-022-00985-3.

Safaeian, S., S. Falahatkar, and M. J. Tourian (2023): Satellite observation of atmospheric CO2 and water storage change over Iran. In: *Scientific Reports* 13.1, pp. 3036–. DOI: 10.1038/s41598-023-28961-x.

Thomas, B. E. O., J. Roger, Y. Gunnell, and S. Ashraf (2023): A method for evaluating population and infrastructure exposed to natural hazards: tests and results for two recent Tonga tsunamis. en. In: *Geoenvironmental Disasters* 10.1, p. 4. DOI: 10.1186/s40677-023-00235-8.

Tourian, M. J., F. Papa, O. Elmi, N. Sneeuw, B. Kitambo, R. M. Tshimanga, A. Paris, and S. Calmant (2023c): Current availability and distribution of Congo Basin's freshwater resources. In: *Communications Earth and Environment* 4.1, pp. 174–. DOI: 10.1038/s43247-023-00836-z.

Tourian, M. J., P. Saemian, V. G. Ferreira, N. Sneeuw, F. Frappart, and F. Papa (2023d): A copula-supported Bayesian framework for spatial downscaling of GRACE-derived terres-

trial water storage flux. In: *Remote Sensing of Environment* 295, p. 113685. DOI: `10.1016/j.rse.2023.113685`.

Wang, B. and N. Sneeuw (2023): Crossover Adjustment of ICESat-2 Satellite Altimetry for the Arctic Region. In: *Advances in Space Research*. DOI: `10.1016/j.asr.2023.07.041`.

Yi, S., P. Saemian, N. Sneeuw, and M. J. Tourian (2023c): Estimating runoff from pan-Arctic drainage basins for 2002–2019 using an improved runoff-storage relationship. In: *Remote Sensing of Environment* 298, p. 113816. DOI: `10.1016/j.rse.2023.113816`.

Conference Presentations

Bützler, C., T. Forbiger, W. Zürn, R. Widmer-Schnidrig, and N. Sneeuw (2023a): *Systematical errors of superconducting gravimeters. An investigation of sensor differences of four dual sphere superconducting gravimeters*. DGG Jahrestagung. Bremen, Germany.

Bützler, C., T. Forbiger, W. Zürn, R. Widmer-Schnidrig, and N. Sneeuw (2023b): *G04p-002: Systematical errors of superconducting gravimeters – An investigation of sensor differences of dual sphere superconducting gravimeters*. IUGG. Berlin, Germany.

Camici, S., L. Brocca, C. Massari, A. Tarpanelli, N. Sneeuw, and et al. (2023): *Potential of NGGM MAGIC for global runoff estimation: the STREAM approach*. MAGIC Science and Applications Workshop 2023. Assisi, Italy.

Deng, X. (2023c): *Gravitational curvatures for a tesseroid and spherical shell with arbitrary order polynomial density*. EGU General Assembly 2023. Vienna, Austria and Online. DOI: `10.5194/egusphere-egu23-3881`.

Deng, X. and N. Sneeuw (2023b): *Superposition error elimination effect of a spherical shell and a spherical zonal band discretized into tesseroids in gravity field modeling*. IUGG. Berlin, Germany. URL: `10.57757/IUGG23-1067`.

Elmi, O., M. J. Tourian, P. Saemian, F. Papa, and N. Sneeuw (2023a): *Long Term Analysis of Global Surface Water Volume Change Using Remote Sensing Data*. Hydrospace 2023. Lisbon, Portugal.

Elmi, O., M. J. Tourian, P. Saemian, and N. Sneeuw (2023b): *Extending river discharge time series of the Global Runoff Data Center (GRDC) using satellite data: A product with uncertainty estimate*. Hydrospace 2023. Lisbon, Portugal.

Foster, J., B. A. Brooks, M. A. Zumberge, S. C. Webb, T. L. Ericksen, J. B. DeSanto, C. D. Chadwell, S. L. Nooner, B. Thomas, and D. A. Schmidt (2023a): *Errors estimates for GNSS-Acoustic measurements of the Alaska-Aleutian subduction zone [INVITED]*. IUGG. Berlin, Germany. DOI: `10.57757/IUGG23-2749`.

Foster, J., M. J. Tourian, P. Saemian, and X. Deng (2023b). Alexander von Humboldt-Stiftung Netzwerktagung am Geodätischen Institut der Universität Stuttgart. Stuttgart, Germany.

Karamzadeh Toularoud, N., Y.-J. Gao, J. Azzola, T. Forbriger, R. Widmer-Schnidrig, E. Gaucher, and A. Rietbrock (2023): *Local earthquake recordings using Distributed Acoustic Sensing (DAS) at BFO*. EGU General Assembly 2023. Vienna, Austria and Online. DOI: `10.5194/egusphere-egu23-16307`.

Ke, S., M. Tourian, and N. Sneeuw (2023): *Estimation of River Discharge using SWOT: full catchment coverage with optimal space and time resolution*. SWOT Science Team Meeting. Toulouse, France.

Ke, S., M. Tourian, N. Sneeuw, R. Paiva, M. Durand, and C. David (2023): *Estimating Daily Discharge of an Entire River Network Using Space-based SWOT Observations*. IUGG. Berlin, Germany.

Liu, B., X. Zou, S. Yi, N. Sneeuw, J. Li, and J. Cai (2023): *Reconstructing GRACE-Like Time Series of High Mountain Glacier Mass Anomalies Based on A Statistical Model*. IUGG. Berlin, Germany.

Sneeuw, N., M. Tourian, and S. Yi (2023): *Total Drainable Water Storage (TDWS): latent hydrological signal in the gravity mean field*. MAGIC Science and Applications Workshop 2023. Assisi, Italy.

Tourian, M., S. Ke, O. Elmi, A. AghaKouchak, D. Gyawali, P. Schollmeier, and B. Wang (2023a). Hydrogeodesy Workshop. Institute of Geodesy, Universtiy of Stuttgart.

Tourian, M., P. Saemian, V. Ferreira, N. Sneeuw, F. Frappart, and F. Papa (2023b): *A copula-supported Bayesian framework for spatial downscaling of GRACE-derived terrestrial water storage flux*. IUGG. Berlin, Germany.

Widmer-Schnidrig, R. and W. Zürn (2023): *How seismometers tilt in response to atmospheric pressure variations: the case of the Hunga Tonga Lamb wave*. eng. IUGG. Berlin, Germany. DOI: `10.57757/IUGG23-2918`.

Yi, S., P. Saemian, N. Sneeuw, and M. Tourian (2023a): *Estimating runoff from pan-Arctic drainage basins for 2002-2019 using and improved runoff-storage relationship*. The 8th Youth Geoscience Forum. Wuhan, China.

Yi, S., P. Saemian, N. Sneeuw, and M. Tourian (2023b): *Estimating runoff from pan-Arctic drainage basins for 2002-2019 using and improved runoff-storage relationship (2)*. Workshop on Geodesy and Climate Change. Zhuhai, China.

Yin, Z., N. Sneeuw, and K. Zhang (2023): *The geometrical features of a gravitational plumb line using the potential flow theory – a revisit*. IUGG. Berlin, Germany.

Theses

(`https://www.gis.uni-stuttgart.de/forschung/dissertationen/`)

Saemian, Peyman: Analyzing and characterizing spaceborne observation of water storage variation

Master Theses

(`https://www.gis.uni-stuttgart.de/lehre/abschlussarbeiten/`)

Knogl, Robin: Ionospheric Detection of Tsunamis from ship-based GNSS

Schneider, Nicholas: Understanding the limitations of Sentinel-3 inland altimetry by validating its measurements over the Rhine River

Schollmeier, Philipp: Understanding the hydrological signature in gravity data

Yu, Ziqing: Validating Sentinel 3 altimetry over the Neckar River using GNSS Interferometric Reflectometry

Bachelor Theses

(`https://www.gis.uni-stuttgart.de/lehre/abschlussarbeiten/`)

Zeng, L: Transboundary water conflicts: the geodetic monitoring approaches

Activities in National and International Organizations

Keller W.

Sneeuw N.
　　Member of ESA Next Generation Gravity Mission (NGGM) Mission Advisory Group (MAG)
　　Professor h.c. (Luojia chair), Wuhan University, China
　　Adjunct Professor of the College of Engineering, University of Tehran, since 2015
　　Fellow International Association of Geodesy (IAG)
　　Full Member Deutsche Geodätische Kommission (DGK)
　　Member of Gauss-Gesellschaft e.V., since 2018
　　Member of the editorial board of Surveys in Geophysics

Tourian M.
　　Chair of IAG ICCC working group on Hydrological loading: measuring and modeling

Research stays

Thomas B.
　　Visiting PhD student at University of Hawaiʻi to realize fieldwork of roving GNSS occupations on Kīlauea volcano with collaboration with the Hawaiʻi Volcano Observatory. (01.2023–04.2023)

Courses – Lecture/Lab/Seminar

Bachelor Geodesy and Geoinformatics (German):

Amtliches Vermessungswesen und Liegenschaftskataster (Grams)	2/0/0/0
Einführung Geodäsie und Geoinformatik (Sneeuw)	2/2/0/0
Integriertes Praktikum/Integrated Field Work (Sneeuw, Foster)	10 days
Landesvermessung (Foster, Thomas)	2/2/0/0
Physikalische Geodäsie (Sneeuw, Beck)	2/2/0/0
Referenzsysteme (Sneeuw, Antoni, Beck)	2/2/0/0
Satellitengeodäsie (Sneeuw, Douch)	2/2/0/0

Master Geodesy and Geoinformatics (German):

Aktuelle Geodätische Satellitenmissionen (Sneeuw)	2/2/0/0
Amtliche Geoinformation (Heß)	2/0/0/0
Ausgewählte Kapitel der Parameterschätzung (Tourian, Douch)	2/2/0/0
Geodätische Erdbeobachtungen (Tourian)	2/0/0/0
Geodynamische Modelle (Engels, Beck)	2/2/0/0
Hydrogeodäsie (Tourian, Saemian)	2/2/0/0
Koordinaten- und Zeitsysteme in der Geodäsie (Sneeuw)	2/0/0/0
Marine-Geodäsie (Foster, Thomas)	2/2/0/0
Physikalische Geodäsie (Engels, Beck)	2/1/0/0
Satellitengeodäsie (Tourian, Douch)	2/1/0/0

Master Umweltschutz (German):

Fernerkundung der Hydrologie und Wasserwirtschaft (Tourian)	2/2/0/0

Master GeoEngine (English):

Advanced Mathematics (Foster, Thomas)	3/2/0/0
Foundations of Satellite Geodesy (Sneeuw, Douch)	2/1/0/0
Integriertes Praktikum/Integrated Field Work (Sneeuw, Foster)	10 days
Map Projections and Geodetic Coordinate Systems (Foster, Thomas)	2/1/0/0
Physical Geodesy (Sneeuw, Beck)	2/1/0/0
Satellite Geodesy Observation Techniques (Foster, Thomas)	2/1/0/0
Statistical Inference (Tourian, Douch)	2/1/0/0

Master Water Resources Engineering and Management (English):

Measurements in the Watercycle (Huisman, Seidel, Widmer-Schnidrig)	4/0/0/0

Institute of Navigation

Breitscheidstraße 2
D-70174 Stuttgart
Tel.: +49 711 685 83400
Fax: +49 711 685 82755
ins@ins.uni-stuttgart.de
http://www.ins.uni-stuttgart.de

Management

Head of Institute, Dean of Studies (since Oct. 2021):	Prof. Dr. techn. Thomas Hobiger
Deputy:	Dr.-Ing. Aloysius Wehr (until Dec. 2023)
Secretary:	Mina Sungur
Retired Professor:	Prof. i.R. Dr.-Ing. Alfred Kleusberg

Academic Staff

M.Eng. Vanessa Bär (from Sep. 2023)	Digital Electronics
Dipl.-Ing. Doris Becker	Navigation Systems
Dipl.-Ing. (FH) Martin Thomas (until Jul. 2023)	Digital Electronics and Hardware Programming
Dr.-Ing. Aloysius Wehr	Optical and Wireless Communication

PhD students

M.Sc. Kevin Gutsche	Precise orbit determination
M.Sc. Shengping He	GNSS troposphere & PPP
M.Sc. Tomke Jantje Hobiger	Parameter Estimation in Dynamic Systems
M.Sc. Daniel Klink	FPGA design, autonomous flight
M.Sc. Marcel Maier	Navigation Software Development
M.Sc. Clemens Sonnleitner	Autonomous flight, ADS-B
M.Sc. Bayram Stucke	Precise orbit determination
M.Sc. Thomas Topp	Navigation Software Development
M.Sc. Rui Wang	GNSS, RTK, PPP, Integrity

IT

Regine Schlothan	Computer infrastructure and programming

Electr. and Mech. Workshop (ZLW)

Dr.-Ing. Aloysius Wehr (until Dec. 2023)	Head of ZLW
Michael Pfeiffer (until Jun. 2023)	Mechanician Master
Sebastian Schneider	Electrician
Dipl.-Ing. (FH) Martin Thomas (until Jul. 2023)	Electrical engineer

External lecturers

Dr. Toni Caesperlein	Dr. Koch Immobilienbewertung, Esslingen

Preface

This report summarizes the activities of the Institute of Navigation (INS) in the year 2023.

Looking back on the past year we can state that we definitely saw very positive developments in many of our research projects, some of them are also being highlighted in this report. We also increased our efforts to write proposal which were submitted to different funding agencies and are currently being reviewed. Maybe the biggest highlight concerning the acquisition of highly competitive funding, was the successful evaluation of the DFG-funded Collaborative Research Centre "ATLAS" to which we are going to contribute with one sub-project from 2024. We also saw several projects reaching their nominal end and we are very happy that we could acquire funding so that the initiated research activities could continue in follow-on projects. The outcome of our research has not only become visible in different reviewed publications and reports, but found its recognition by two awards which were presented by two of our PhD students. Clemens was presented an "Outstanding presentation award" at the European Navigation Conference 2023 for his ground-breaking work on making airspace surveillance possible with low-cost hardware. Kevin, who attended the ION's GNSS+ conference in fall 2023 received "Best Presentation Award" for his work on "Addressing Inaccurate Phase Center Offsets in Precise Orbit Determination for Agile Satellite Missions".

In terms of teaching, we finalized our internal Git repository that includes now all lecture materials in LaTeX and we revised the contents of the "Measurement Techniques II" in order to equip our students with the necessary basic skills concerning electrical engineering and electronics. Facing significantly lower course students than in the years before required to optimize our course program and offer courses to those interested even when the required minimum number of students could not be reached.

Concerning staffing, the year 2023 was one in which we saw three of our colleagues entering retirement. We wish them all the best for their new stage of life and face the situation that they left a void which will take some time to be filled.

Prof. Dr. Thomas Hobiger
(Head of the Institute of Navigation)

Research

The INS identifies new fields of applications, develops and tests navigation solutions, and assigns research projects according to four "focus areas", which were originally defined in 2018. Considering the way the institute is organized and its participation in different research projects, those areas reflect most of the activities of the INS. Moreover, the teaching activities, which are described later in this report, also reflect the research activities that the INS is involved in. Figure 1 depicts those focus areas, which are grouped around the topics of "positioning, navigation, and timing".

Figure 1: INS focus areas to which the institute is actively contributing in the form of research projects.

While most of the current research projects can be clearly assigned to one or two focus areas shown in the figure, larger research projects, described later in this report, usually fall under the category "applications" but require intense input from the other three research areas. In the following, the purpose and vision for each research area are presented alongside examples of ongoing research projects.

Research focus: Theory

The following sections describe theoretical work that was conducted in 2023.

ADS-B

The Automatic Dependent Surveillance - Broadcast (ADS-B) standard allows airspace operators to monitor their area of responsibility with a high precision and update rate in a very cost efficient way. As is is a quite old protocol, without any modern security measurements in mind, it is prone to attacks which can degrade the airspace security and potentially lead to fatal accidents. Wide-Area Multilateration (WAM) systems, that can mitigate these attack vectors, are usually very expensive and require a complex clock synchronization.

At the institute we investigate a novel approach in which additionally to the aircraft position and velocities the relative clock offsets of the receivers are estimated in an Extended Kalman Filter (EKF). First simulation results, that were presented at the ENC2023, indicate that the system performs very well and might remove the requirement of an external clock synchronization. In Figure 2 some results of a simulation for the German airspace and aircraft trajectories based on data from the OpenskyNetwork are given.

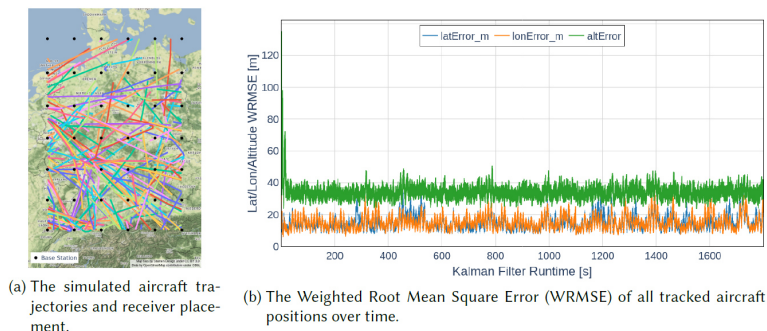Further work will focus on spoofer and outlier detection and the scalability of the system.

(a) The simulated aircraft trajectories and receiver placement.

(b) The Weighted Root Mean Square Error (WRMSE) of all tracked aircraft positions over time.

Figure 2: ADS-B MLAT simulation setup and results.

Robust Kalman filtering and integrity monitoring for GNSS positioning

Based on the enhanced performance of RTK algorithms in robust Kalman filtering referring to Wang et al. (2023), the robust estimation is further applied to PPP applications. In the continuing work, we focus not only on the adjustment of the measurement noise matrix in stochastic modeling, but also on the confidence domain of estimated states, which is expected to contain the so-called true value under a pre-defined Integrity Risk (IR). Therefore, we exploit the interval bounding analysis for a more realistic assessment of GNSS measurement uncertainties and propagate them from the range-domain into the state-domain. In practice, GNSS measurements are inevitably contaminated by outliers (e.g., multipath effects), resulting in a degradation of Kalman filtering.

Thus, we utilize the polytope-based bounding method for quality control in both pseudorange and carrier-phase measurements. In the fault detection procedure, this polytope bounding method enables to offer geometric constraints by means of the convex optimization. Once an outlier exists, i.e., the remaining residual is beyond the interval error bound, which is derived by a specified IR, the polytope solution can yield an empty set in such faulty case. This property is similar but superior to the classical fault detection commonly using the Chi-square test.

The comparison of these two fault detectors and their performances was shortly presented at the ENC conference. Figure 3 illustrates an example of two bounding methods (i.e., zonotope and polytope) in the interval bounding analysis. Unlike the polytope boundary taking measurement residuals into account, the shape of the zonotope is always centred at the estimated position, and relies only on the satellite geometry and the interval error bound. Subsequently, the polytope bounding method is integrated into a designed Receiver Autonomous Integrity Monitoring (RAIM) framework based on a robust Kalman filter, which involves the protection level computation as well. To validate the effectiveness of this complete RAIM framework, multiple scenarios with simulated and real data have been conducted. The relevant research paper is considered to be submitted to an academic journal in 2024.
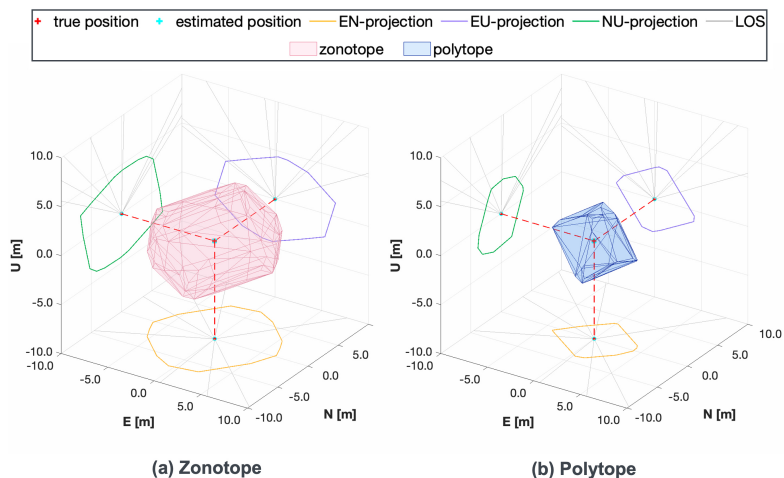
Figure 3: 3D example with respect to the zonotope and polytope solution

Measurement fusion using co-located receivers for improving GNSS meteorology

In 2023, we refined the fusion algorithm on the observation level for the Zenith Wet Delay (ZWD) estimation, and developed a novel model to provide common ZWD estimates on a local scale for our joint Polish-German research project "Simultaneous Troposphere Estimation with Precise Point Positioning" (STEPPP), funded by Deutsche Forschungsgemeinschaft (DFG). The related research has been reported at the EGU conference and submitted to an academic journal with a current status of undergoing review. Considering that tropospheric estimation is prone to be limited due to receiver noises and systematic biases, the proposed fusion model is intended to estimate one common ZWDparameter with less noise for co-located receiver sites.

According to experimental results from simulations and low-cost GNSS receiver field tests, the fusion model outperforms the single receiver PPP model in terms of precision, accuracy and noise level in tropospheric estimation. As depicted in figure 4 for investigating the stability of Zenith Total Delay (ZTD) time series by the overlapping Allan deviation (ADEV), when averaging out more stochastic processes, the fusion curve gradually converges towards the reference curve of Near Real-Time (NRT) ZTDs, and both are more stable than the radiometer curve. On the basis of this fusion approach, further study is in progress.
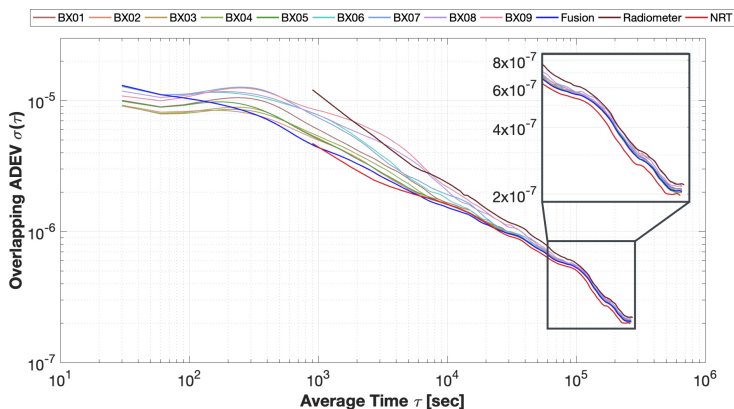
Figure 4: Low-cost demonstration test for 13 days with respect to reference values from the radiometer and NRT ZTDs

Multi-Receiver Precise Baseline Determination

Within the last year, we finished our development on the Multi-Receiver Precise Baseline Determination (MR-PBD) and published it in the Proceedings of the 36th International Technical Meeting of the Satellite Division of The Institute of Navigation (ION GNSS+ 2023) (Stucke et al. (2023)). The developed algorithm is capable of fusing the observations of multiple receivers distributed on two spacecraft to a single estimator. We were able to recover extremely precise baselines using this algorithm. Using the MR-PBD, we performed a simultaneous estimation of the inter-spacecraft baseline with either each attitude of the spacecraft or each lever arm of the antennas. This simultanous estimation was not possible before. We analyzed the simultaneous estimation of the inter-spacecraft baseline and both attitudes of the spacecraft and presented the outcomes at the ION GNSS+ 2023 (Stucke et al. (2023)). Figure 5 depicts the improve of the accuracy of the baseline estimate with an increasing number of antennas mounted on each spacecraft. The results of the simultaneous estimation of the inter-spacecraft baseline and the antenna off-sets of all included antennas were presented at the German Aerospace Congress (DGLRK 2023) (Stucke et al. (2023)). However, the algorithm appears to diverge if all three of the parameters, the baseline, the attitudes, and the antenna off-sets are estimated at once.
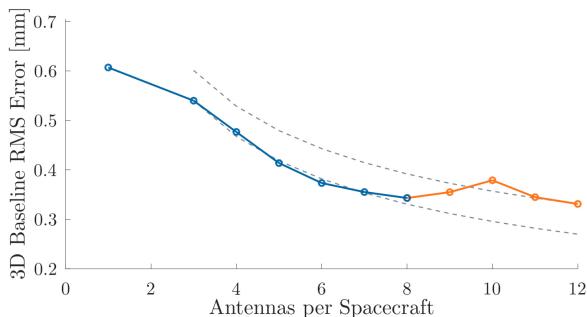
Figure 5: 3D RMS of an inter-spacecraft baseline over the number of included antennas per spacecraft

Research focus: Software development

The following sections describe the institute's software development activities in the year 2023.

INSTINCT - INS Toolkit for Integrated Navigation Concepts and Training

After making INSTINCT available to the public last year on GitHub[1], development progressed steadily. New algorithms like an INS/GNSS Tightly-coupled Kalman Filter (TCKF) were developed. Furthermore, the Real-Time Kinematic algorithm is approaching it's final stages of testing and will be released in a big update later in 2024 on GitHub. The documentation will also receive a big overhaul to explain better how to use the software to users and developers.

Apart from algorithms, there were a lot of other improvements. Figure 6a shows the new event system. Algorithms can raise events which can be directly shown in the plots. This provides an easy way to spot problems during algorithm development. When comparing position solutions, it's quite hard to see improvements in plots such as figure 6a. That is why INSTINCT now can plot the difference between solutions, which is shown in figure 6b. The innovative part about this is, that it also works with signals at different data rates. Interpolation of the data is automatically performed in a way which reduces interpolation errors without any need for user input.

Another feature implemented during last year which will be released in the next update is an ublox file reader, so ublox GNSS observations as well as navigation data can be read and used in navigation algorithms. Moreover the ublox observations can be fed into another new node, the RINEX data logger, to write out RINEX obs files. With this, ublox to RINEX conversions can be performed closing a big gap in GNSS processing tooling, as such converters are not widely available.

---

[1] https://github.com/UniStuttgart-INS/INSTINCT

If you want to stay informed about the development of INSTINCT and not miss updates, please feel free to start the GitHub repository. GitHub releases with changelogs and precompiled executables are planned, so it is worth adding the repository to the watch list to get notified when the update is happening.
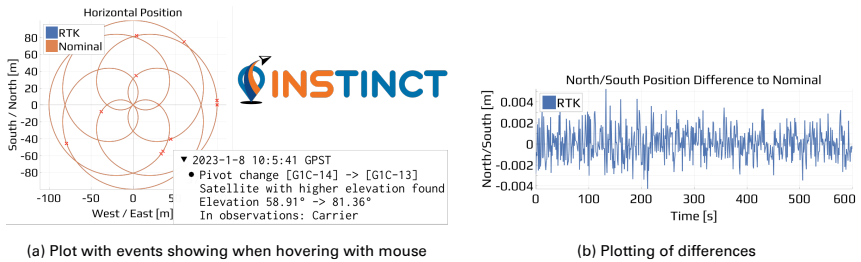

(a) Plot with events showing when hovering with mouse

(b) Plotting of differences

Figure 6: New features of INSTINCT

PODCAST - Precise Orbit Determination for Complex and Agile Satellite Technology

POD - Precise Orbit Determination

Within the last year, significant progress was achieved with respect to the Precise Orbit Determination (POD) of non-agile and agile satellites. First, the modeling of the forces that Low Earth Orbit (LEO) satellites experience in orbit was partially reworked and fully validated. Additional changes include time-variable gravity potentials, new tide models, as well as highly precise non-gravitational models based on ray-tracing. Figure 7 depicts the error of the orbit propagation of Sentinel-6A for 24h in radial, along-track, and cross-track direction. This demonstrates the good performance and validity of the implemented models.
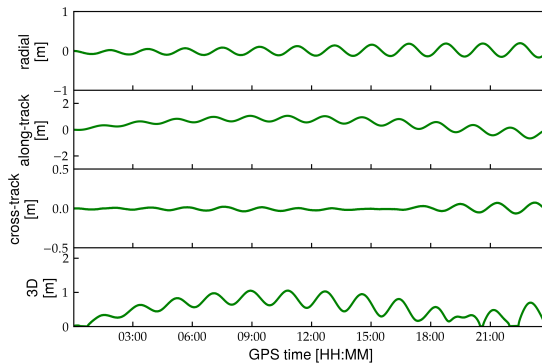

Figure 7: Error in the fully propagated trajectory of Sentinel-6A compared to the POD solution.

The POD of agile satellites was investigated in-depth based on HIL simulations and realistic missions scenarios. The main results of this study were presented at the ION GNSS+ 2023 (Gutsche et al. 2023). Additionally, the POD of agile satellites was demonstrated using a low-cost GNSS receiver (Gutsche et al. 2023).

Finally, the POD of non-agile satellites was further validated based on in-orbit data from both Sentinel-3 and Sentinel-6. The improvements in the software lead to a significant reduction in the estimation error, which is now below 2 cm 3D RMS. Figure 8 displays this error in radial, along-track, and cross-track direction for Sentinel-6A.
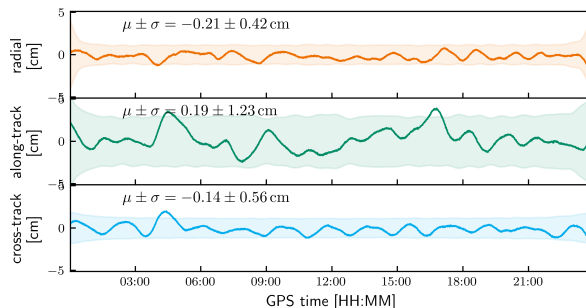

Figure 8: Estimation error of Sentinel-6A with respect to the solution of the Copernicus POD Quality Working Group on 19th of November 2021.

PBD - Precise Baseline Determination

The precise baseline determination part within our in-house estimator PODCAST was enhanced by algorithms of the MR-PBD introduced in the subsection Multi-Receiver Precise Baseline Determination. Furthermore, the development of the PBD solution is at the final stage. The validation with in-orbit data is coming in the first quarter of 2024.

Development of a new mapping function for troposphere studies

To overcome the limitations in the traditional two-axis gradient model, we proposed the B-spline Mapping Function (BMF) as an alternative to represent the asymmetry of the tropospheric delay. After experimental verification with a large amount of data, BMF turns out to have the following advantages:

- It can improve the repeatability of PPP positioning results, whereby the repeatability is about twice as high as with the gradient model. Under extreme weather conditions, this improvement is even higher.

- BMF can significantly reduce the correlation between weather conditions and positioning accuracy, which leads to weaken the adverse impact of extreme weather conditions on the positioning accuracy.

- BMF can normalize the distribution of post-fit residuals and make it closer to Gaussian distribution. After applying the azimuth-dependent weighting model, BMF can accelerate the convergence time of PPP.

- BMF can provide rich atmospheric information, allowing the tropospheric gradient to be expanded into divergence to more accurately describe tropospheric asymmetry.

In figure 9 representative BMF results in comparison with results of standard strategies, e.g. NONE (no troposphere model), GRAD (two-axis gradient model) and GRD2 (2nd-order gradient model) are given.
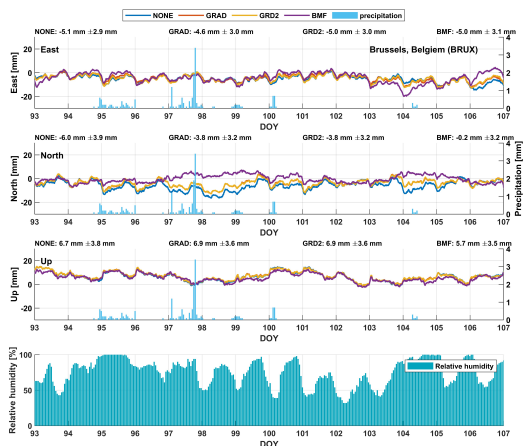

Figure 9: Coordinate time series of IGS stations in Brussels, Belgium (BRUX, upper) during 2.Apr. - 16.Apr, 2022. Right y-axis refers to the hourly-average precipitation during the timespan. The accuracies are shown in "NAME: bias ± uncertainty"

Sensor fusion of multiple inertial measurement units

Urban air mobility has stringent requirements on accuracy, reliability and integrity of a navigation solution, while also keeping costs low. Therefore, a fusion algorithm for multiple low-cost inertial measurement units (IMUs) was developed. In our approach, the IMUs are fused by assuming acceleration and angular rate as integrated random walk processes. Additionally, relative biases between each IMU and a reference IMU are estimated. Figure 10 shows the corresponding filter architecture. As can be seen, the IMUs receive a common time stamp from GPS. This is necessary for synchronization of the IMUs. Each IMU provides specific force and angular rate measurements to the "Multi-IMU Fusion Filter". The output of the fusion filter is virtually the same as from a single-IMU, which is therefore called "Virtual IMU" (VIMU). Its output is then fed into a Tightly Coupled Kalman Filter (TCKF), where it is fused with GPS observations to calculate a navigation solution.
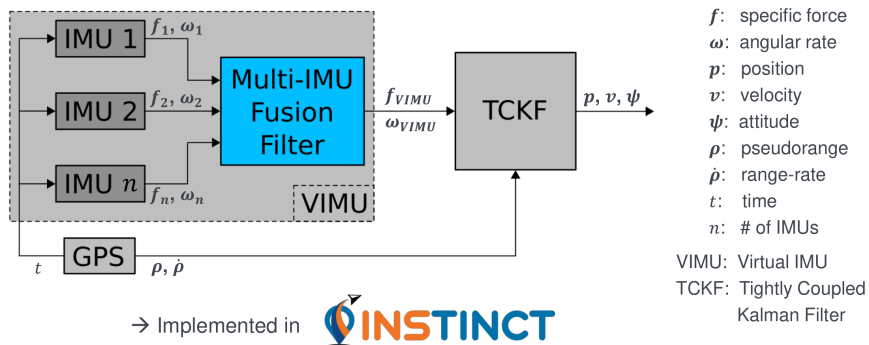
Figure 10: Multi-IMU filter architecture.

This filter architecture was implemented in INSTINCT and validated in simulation at first, using GPS observations generated by the institute's Spirent SimGEN simulator.

Research focus: Applications

The following sections describe applications on which the INS worked on in the year 2023.

Flight Test with the multiple inertial measurement unit setup

After the successful validation of the multiple inertial measurement unit concept, flight tests were performed. The test setup consisted of:

- Multi-IMU: consisting of five identical low-cost IMUs (developed at the institute)

- VectorNav VN310E: high-grade IMU as a reference

- Emlid Reach RS2 + M2: post-processed kinematics, also as a reference

These sensors and receivers were flown on the institute's Prism Coaxial X8 drone at the Ihinger Hof. The gathered data were then post-processed in INSTINCT, where the TCKF-VIMU solution is compared to another solution with the TCKF, that is calculated using only a single-IMU of the Multi-IMU array.

Figure 11 shows the altitude and the altitude error of the test flight. The latter shows the differences of each TCKF solution to the PPK solution. After take-off the TCKF solutions converge quickly and both, the VIMU and single-IMU cases, are close to the PPK solution. Comparing the position errors, the TCKF-VIMU is in Lat/Lon/Alt better than the TCKF-single-IMU by 2% / 1% / 3%. Despite the slightly reduced position errors, the Multi-IMU's filter architecture is resilient regarding the loss of one of the low-cost IMU.
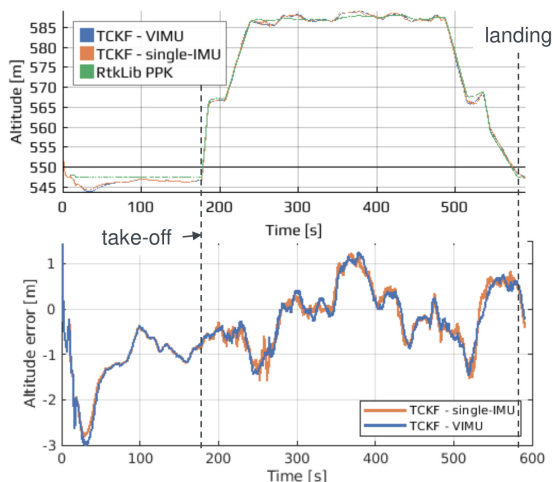
Figure 11: Altitude and altitude error of TCKF-VIMU and TCKF-single-IMU.

List of Publications

Gutsche K., Hobiger T., Winkler S.: Addressing Inaccurate Phase Center Offsets in Precise Orbit Determination for Agile Satellite Missions, Proceedings of the 36th International Technical Meeting of the Satellite Division of The Institute of Navigation (ION GNSS+ 2023), 3082-3095, Denver, USA.

Stucke M.B., Hobiger T., Möller G, Gutsche K., Winkler S,: Multi-Receiver Precise Baseline Determination: Coupled Baseline an Attitude Estimation with a Low-Cost Off-The-Shelf GNSS Receiver, Proceedings of the 36th International Technical Meeting of the Satellite Division of The Institute of Navigation (ION GNSS+ 2023), 3082-3095, Denver, USA.

Wang R., Becker D., and Hobiger T.: Stochastic modeling with robust Kalman filter for real-time kinematic GPS single-frequency positioning, GPS Solutions, vol. 27, no. 3, p. 153, 2023.

List of Presentations

Gutsche K., Hobiger T., Möller G, Winkler S.: Precise Orbit Determination of Agile LEO Satellites Using Simulations with a Low-Cost Commercial Off-the-Shelf Receiver, German Aerospace Congress (DLRK) 2023, Stuttgart, Germany.

He S., Becker D., Hobiger T.: Modelling asymmetric troposphere delays by means of B-splines, 28th IUGG General Assembly 2023, Berlin, Germany.

Maier M., Hobiger T., Topp T. and Thomas M.: Resilient navigation through a novel fusion approach for multiple inertial measurement units, European Navigation Conference 2023, Noordwijk, Netherlands.

Stucke M.B., Hobiger T., Möller G, Gutsche K., Winkler S: Exploitation of a Low-Cost Off-The-Shelf GNSS Receiver for Coupled Baseline and Attitude Estimation, German Aerospace Congress (DLRK) 2023, Stuttgart, Germany.

Wang R., Becker D., and Hobiger T.: Interval bounding analysis for precise point positioning, European Navigation Conference 2023, Noordwijk, Netherlands.

Wang R., Becker D., and Hobiger T.: Stochastic modeling with robust Kalman filter for real-time kinematic GPS single-frequency positioning. GPS Solutions, 27(3), Article 3. https://doi.org/10.1007/s10291-023-01479-5.

Wang R., Hobiger T., Marut G., and Hadas T.: Improving GNSS meteorology by fusing measurements of multi-receiver sites on the observation level, EGU General Assembly 2023, Vienna, Austria.

Activities in National and International Organizations

Prof. Hobiger Editorial board member "Acta Geodaetica et Geophysica"
    Member of the German Geodetic Commission
    Corresponding member of the Austrian Geodetic Commission
    Fellow of the International Association of the Geodesy
    Member of the Institute of Navigation
    Member of the Royal Institute of Navigation
    Member of the German Institute of Navigation
    Member of the American Geophysical Union

Prof. Kleusberg Fellow of the International Association of the Geodesy
    Member of the Institute of Navigation
    Member of the Royal Institute of Navigation
    Member of the German Institute of Navigation

Teaching and Supervision

During the past year, the downward trend in the number of students in the three geodesy degree programs has unfortunately continued. This has various effects on the form of teaching. In foundation courses with few participants, students have an excellent student-to-staff ratio. Elective subjects offered the opportunity to teach content individually and to support the students. In the navigation specialization module, e.g. we were able to cater specifically to students' wishes and combine the theory of filter techniques with practical exercises on the industry-standard GNSS simulators that are available through Spirent's Academia Programme and Orolia's Academic Partnership Program. Ideas on navigation topics were

developed to give geodesy students an insight into non-standard disciplines. This allowed a small group to focus specifically on signal propagation and antenna technology, topics that are essential in the practice of navigation. In future, the focus will be on skills in electronics and electrical engineering.

The following parts of this section list student thesis projects which were completed in 2023 and summarize the teaching activities of the institute.

Master Theses

Ghribi, Adam: Adaptive Kalman Filtering for Precise Orbit Determination of Low Earth Satellites (Supervisor: K. Gutsche)

Lauterbach, Mike: Evaluation von RTK-Szenarien durch Generation an verschiedenen GNSS-Simulatoren (Supervisor: D. Becker)

Seyfried, Michael: Echtzeit-Charakterisierung von IMUs für hochgenaue Sensorfusionsalgorithmen (Supervisors: M. Maier, T. Topp)

Education - Lectures/Exercises

Bachelor Geodesy & Geoinformatics

Adjustment Theory I (Hobiger, Becker)	2/1
Adjustment Theory II (Hobiger, Becker)	2/1
Fundamentals of Navigation (Hobiger, Becker, Stucke)	2/2
Integrated Fieldwork (Sonnleitner, Topp)	10 days
Introduction of Geodesy and Geoinformatic (Hobiger, Becker)	2/2
Measurement Techniques II (Wehr, Sonnleitner, Klink)	2/2
Valuation (Caesperlein)	1/0

Master Geodesy & Geoinformatics

Filtering Techniques (Hobiger, Topp)	1/1
Inertial Navigation (Hobiger, Topp)	1/1
Inertial Sensors (Hobiger)	1/0
Integrated Navigation (Hobiger, Topp, Becker)	1/1
Measurement Techniques in Navigation (Wehr, Klink)	1/3
Satellite Navigation (Hobiger, Becker, Gutsche)	1/1
Signal Propagation and Antenna Theory (Hobiger, Becker, Klink)	1/1
State Estimation in Dynamic Systems (Hobiger, Maier, Gutsche)	2/1
Object-oriented Programming in C++ (Hobiger, Sonnleitner, Topp)	1/3
Property Valuation (Caesperlein)	1/0
Simultaneous Localization and Mapping (SLAM) (Hobiger, Maier, Klink)	1/1

Master GeoEngine

Dynamic System Estimation (Hobiger, Maier, Stucke)	2/1
Integrated Positioning and Navigation (Hobiger, Topp)	2/1
Satellite Navigation (Hobiger, Becker, Stucke)	2/1

Master Aerospace Engineering

Inertial Navigation (Hobiger)	2/0
Satellite Navigation (Hobiger)	2/0

Master Electromobility

Navigation of Surface Vehicles (Becker)	2/0
Satellite Navigation (Hobiger)	2/0

Institute for Photogrammetry and Geoinformatics

Geschwister-Scholl-Str. 24D
D-70174 Stuttgart
Tel.: +49 711 685 83336
Fax: +49 711 685 83297
info@ifp.uni-stuttgart.de
http://www.ifp.uni-stuttgart.de

Management

Head of Institute:	Prof. Dr.-Ing. Uwe Sörgel
Deputy:	apl. Prof. Dr.-Ing. Norbert Haala
Personal Assistants:	Carmen Kaspar
	Ute Schinzel
Emeritus Professor:	Prof. Dr.-Ing. Dieter Fritsch

Academic Staff

M.Sc. David Collmar	Crowd-based Data Collection
Dr.-Ing. Michael Cramer	Photogrammetric Systems
Dipl.-Ing.(FH) Markus Englich	Laboratory, Computing Facilities
apl. Prof. Dr.-Ing. Norbert Haala	Photogrammetric Computer Vision
M.Sc. Lena Joachim (until 5/2023)	Integrative Computational Design
M.Sc. Michael Kölle (until 9/2023)	Crowd-based Data Collection
M.Sc. Dominik Laupheimer	Classification in Remote Sensing
Dr. Lida Pournodrati (since 8/2023)	Bathymetry
M.Sc. Vinvcent Reß (since 9/2023)	Integrative Computational Design
M.Sc. Philipp Schneider (until 7/2023)	SAR Interferometrie
M.Sc. David Skuddies (since 8/2023)	LiDAR SLAM
Dr.-Ing. Volker Walter	Geoinformatics

Stipendiaries and external PhD Students

M.Sc. Jonathan G. Santiago	Multimodal Representation Learning
Dipl.-Phys. Hendrik Schilling	Classification of Hyperspectral Data
M.Sc. Wei Zhang	Visual SLAM for Augmented Reality
M.Sc. Xinlong Zhang	Object Recognition from LiDAR Data

Guest Scientists

M.Sc. Grzegorz Gabara (until 9/2023)   3D Object Reconstruction

External Teaching Staff

Dipl.-Ing. Stefan Dvorak, Amt für Stadtentwicklung und Vermessung, Reutlingen

Research Activities in ifp organized in four thematic Groups

Geoinformatics	Dr.-Ing. Volker Walter
Photogrammetric Computer Vision	apl. Prof. Dr.-Ing. Norbert Haala
Photogrammetric Systems	Dr.-Ing. Michael Cramer
Remote Sensing	Prof. Dr.-Ing. Uwe Sörgel

Research Projects

Optimizing Polygon Integration for Crowdsourced Data (D. Collmar)

Multiple data collection and subsequent data integration is a typical approach to improve the quality of data from paid crowdsourcing. If the collected data is represented by polygons, the integration can be performed with a raster-based approach using binary voting per raster cell. If such a voting is applied, the integration result is strongly influenced by the choice of the integration threshold, which determines how many polygons are required per raster cell in order to include a particular raster cell in the integrated polygon.

A study was conducted in which 115 orthoimage sections - each containing one single tree - were processed by 150 different crowdworkers. An example of an image section can be seen in Figure 1, the 150 acquired polygons are shown in yellow.

In order to find the optimal threshold parameter, the integration was performed for all possible integration threshold values, ranging from 1 to 150. The quality of the resulting integrated polygons was analyzed via intersection over union (IoU) and Hausdorff distance. If you plot and compare the results for different threshold values, it becomes clear that both too large and too small an integration threshold value leads to a poorer quality of the integrated polygon. The optimal integration threshold appears to be around 50%, as can be seen in Figure 2, where the optimal value is achieved through both quality measures.
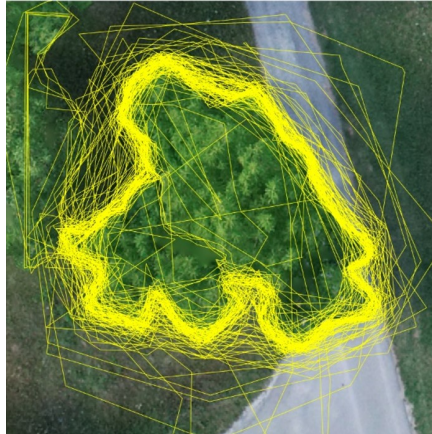
Figure 1: Image section with 150 polygons.

Figure 2 also indicates a saturation effect, making an increase in sample size from 100 to 150 obsolete. Further research proved that applying a filtering process using geometric moments before integration leads to significantly better results, allowing the surpassing of the saturation point. Additionally, filtering by single moments proved to have varying effects on post-integration quality, whereas combining multiple moments in the filtering process appeared to combine their respective effects, allowing for an even higher quality after integration.
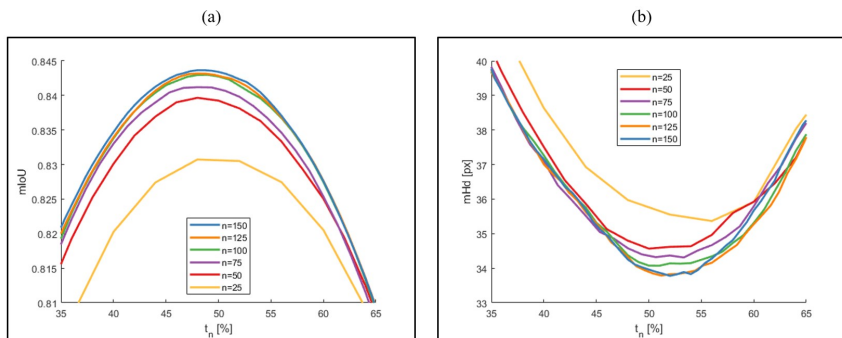

Figure 2: Quality evaluation for selected number of acquisitions n: (a) mean intersection over union (b) mean Hausdorff distance.

AI-supported Collaborative Control and Trajectory Generation of Mobile Manipulators for Indoor Construction Tasks (V. Reß)

Our work in the context of the cluster of Excellence Integrative Computational Design and Construction for Architecture (IntCDC) at the University of Stuttgart is aiming at the monitoring of construction sites. Overarching goal is to harness the potential of digital technologies to manufacturing and construction in the building sector and to enable a direct digital work-flow for data capture, while aiming at the generation of BIM and digital twins. Monitoring construction sites for documentation purposes is an important application scenario for the geodetic capture of 3D point clouds. While in the past, Terrestrial Laser Scanning (TLS) from fixed stations had been state-of-the-art, meanwhile mobile systems applying SLAM-based methods are increasingly used for data collection in such scenarios.

Current visual SLAM methods can provide dense representations reasonably well, but are typically limited to well-textured environments and rather small spaces, such as single rooms, which are typically captured at short measurement distances. In contrast, real-world applications of large indoor scenes like construction sites and factory halls remain challenging.

According to the applied sensor type (see Figure 3), SLAM algorithms are categorised into LiDAR and visual SLAM. LiDAR based approaches apply sensors measuring either as 2D or 3D point clouds. While approaches limited to a planar 2D space are quite mature and already enter consumer market, methods using 3D point clouds are still topic of research. Visual SLAM algorithms apply monocular, stereo or even RGB-D imagery. Compared to LiDAR sensors, cameras are significantly cheaper and therefore enable a much wider range of applications. Furthermore, the analysis of the captured images is not limited to geometric information extraction during localization and mapping. Due to rich information embedded in RGB imagery, visual SLAM is advantageous for visualization purposes and for semantic segmentation of the environment. On the other hand, the sensor principle of typical RGB-D devices limits their application to close range scenarios, while monocular SLAM frequently suffers from scale drift. Even though the angular resolution of LiDAR sensors declines proportional to distance caused by diffraction, in practice, the direct range measurement principle allows for larger scene extent compared to visual SLAM schemes. Further improvements in terms of localization reliability and accuracy for both groups of methods can be achieved by fusion with additional and complementing observations such as IMU or odometer data. In order to support data collection in larger scale environments like construction sites and factory halls, we combine measures both from LiDAR and stereo cameras in our system. As an example, we chose a factory hall, in which we monitor indoor construction activities.

Typical visual SLAM pipelines often result in a point cloud map. However, this format may not be sufficient for robots to localize themselves within the map while navigating collision-free, due to the inherent sparseness of point clouds. Additionally, applications such as first-person navigation through a scene along a newly rendered path require realistic images from novel viewpoints. To overcome these challenges, we have adopted the 3D Gaussian Splatting method for training a radiance field of the scene. This approach utilizes both the estimated poses and the globally consistent point cloud produced in the last stage as initial Gaussian

a) Overview   b) Detail - Cameras   c) Detail - LiDAR

Figure 3: Overview of available sensors.

positions. While following the default configuration, we have made a key enhancement by adding stereo depth for additional supervision, thereby improving geometric reconstruction.

Figure 4 presents an example of input stereo depth, which is often incomplete due to issues like low texture or limited stereo baseline. The depth images rendered using our trained 3D Gaussian model address these difficulties effectively, producing fully complete depths with clearer object borders.
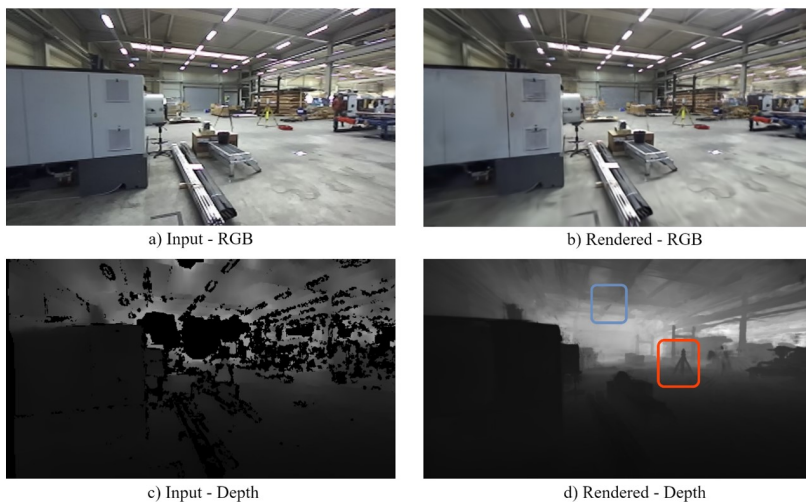

a) Input - RGB   b) Rendered - RGB

c) Input - Depth   d) Rendered - Depth

Figure 4: Comparison of RGB and depth images with those rendered by our 3D Gaussian splatting model.

Enhancing LiDAR Inertial Odometry with Dense Multi Scan Adjustment for Accurate Mapping (D. Skuddies)

Robotic navigation and mapping heavily rely on accurately processing environmental data, typically gathered using Light Detection and Ranging (LiDAR) sensors. Traditional approaches to processing this data involve simplifying point clouds into key features or establishing direct correspondences between data sets, which can limit precision and adaptability in complex or dynamic environments.

We have developed a method that offers an alternative approach to LiDAR data processing for navigation and mapping applications. This method diverges from traditional techniques by avoiding the simplification of point clouds and instead, optimizes the data as a whole. It does so by segmenting the environment into a grid of cells and employing statistical models to iteratively refine the global representation of the space.

The method's primary innovation lies in its handling of LiDAR point clouds. By assigning statistical distributions to grid cells containing LiDAR data points, the algorithm iteratively improves its representation of the environment. This strategy enables effective handling of areas with small overlaps or moving objects without necessitating the identification of specific features or direct point-to-point matching.

To enhance the algorithm's performance, data from Inertial Measurement Units (IMUs), which monitor movement and orientation, are incorporated. This addition improves trajectory tracking, offering greater accuracy and robustness, especially in environments that pose challenges for LiDAR-only methods, such as feature-sparse or highly dynamic areas.

The application of this new method across various settings, including both indoor and outdoor environments, has yielded positive outcomes. It has demonstrated improved accuracy and robustness compared to existing approaches, successfully navigating through areas where other methods struggle. In Figure 5 mapping result of a bicycle sequence is shown.
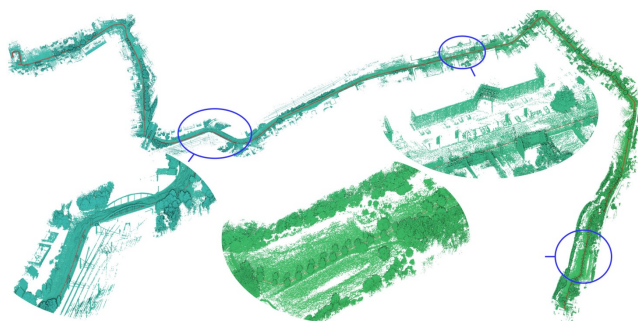

Figure 5: Resulting keyframe point cloud from a bicycle sequence data recording. The scene contains urban areas, field paths and dynamic objects. The trajectory of the sensor platform mounted on a bicycle trailer is marked in red. For areas marked in blue, detail views are provided.

Target-guided Learning for Rare Class Segmentation in Large-Scale Urban Point Clouds (X. Zhang)

In large-scale urban areas, the diversity of objects and the complexity of scenes pose challenges to semantic segmentation of point clouds. In particular, the data imbalance problem often results in poor performance for rare classes in large scenes. We propose a rare class segmentation method based on the target-guided transformer network. In the network, all the feature extraction and segmentation procedures are realized by attention mechanisms. The self-attention blocks are embedded in U-Net-like structure as illustrated in Figure 6 to gradually integrate the features from local to global. Then, under the supervision of our target-guided block, the instance features of data-imbalanced rare classes are mapped onto the multi-scale features. At last, a multi-layer perceptron is utilized to convert the fused features to the segmentation logits for generating the semantic labels.
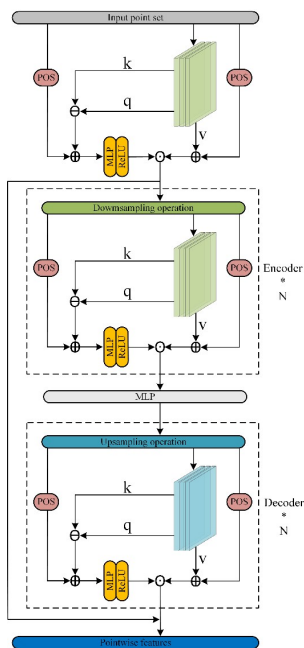

Figure 6: Structure of the self-attention blocks.

As showed in Figure 7, experiments using the Hessigheim High-Resolution 3D Point Cloud Benchmark indicated that our approach considerably outperforms the baseline network by up to 11.66% in terms of mean F1 score. In particular, the rare classes Vehicle and Chimney obtain outstanding F1-scores of 82.40% and 82.51%, respectively. Furthermore, our method achieves an overall accuracy of 87.63%, which increases by 1.09% compared to the baseline model.
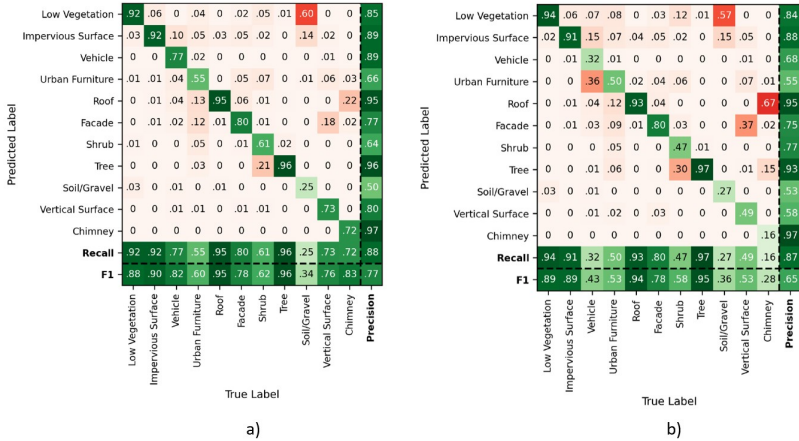
Figure 7: (a) confusion matrix on our network; (b) confusion matrix on baseline model Point Transformer.

BAMF-SLAM: Bundle Adjusted Multi-Fisheye Visual-Inertial SLAM Using Recurrent Field Transforms (W. Zhang)

We present BAMF-SLAM, a novel multi-fisheye visual-inertial SLAM system that utilizes Bundle Adjustment (BA) and recurrent field transforms (RFT) to achieve accurate and robust state estimation in challenging scenarios. First, our system directly operates on raw fisheye images, enabling us to fully exploit the wide Field-of-View (FoV) of fisheye cameras. Second, to overcome the low-texture challenge, we explore the tightly-coupled integration of multi-camera inputs and complementary inertial measurements via a unified factor graph and jointly optimize the poses and dense depth maps. Third, for global consistency, the wide FoV of the fisheye camera allows the system to find more potential loop closures, and powered by the broad convergence basin of RFT, our system can perform very wide baseline loop closing with little overlap. Furthermore, we introduce a semi-pose-graph BA method to avoid the expensive full global BA. By combining relative pose factors with loop closure factors, the global states can be adjusted efficiently with modest memory footprint while maintaining high accuracy.

Evaluations on TUM-VI, Hilti-Oxford and Newer College datasets show the superior performance of the proposed system over prior works. In the Hilti SLAM Challenge 2022, our VIO version achieves second place. In a subsequent submission, our complete system, including the global BA backend, outperforms the winning approach.
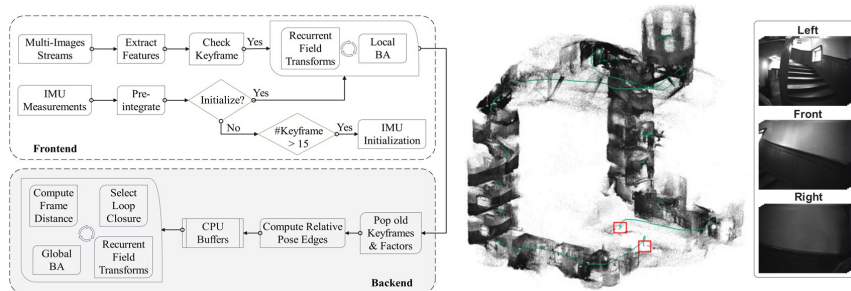
Figure 8: Left: Overview of the proposed system. Right: Estimated point cloud and trajectory by the proposed system on exp09 sequence of Hilti-Oxford dataset. The start and end positions of the trajectory are marked with red rectangles.
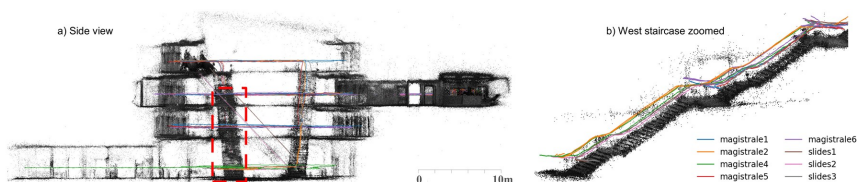

Figure 9: Qualitative results on TUM-VI dataset. Estimated trajectories are depicted in colors and point clouds are accumulated. Red-box marked region is zoomed in on the right from the side look to provide a better illustration. Notably our results demonstrate high consistency in cleanly separating floors and clear-cut edges of stairs.

HI-SLAM: Monocular Real-time Dense Mapping with Hybrid Implicit Fields

We present a neural field-based real-time monocular mapping framework for accurate and dense Simultaneous Localization and Mapping (SLAM). Recent neural mapping frameworks show promising results, but rely on RGB-D or pose inputs, or cannot run in real-time. To address these limitations, our approach integrates dense-SLAM with neural implicit fields. Specifically, our dense SLAM approach runs parallel tracking and global optimization, while a neural field-based map is constructed incrementally based on the latest SLAM estimates. For the efficient construction of neural fields, we employ multi-resolution grid encoding and signed distance function (SDF) representation. This allows us to keep the map always up-to-date and adapt instantly to global updates via loop closing. For global consistency, we propose an efficient Sim(3)-based pose graph bundle adjustment (PGBA) approach to run online loop closing and mitigate the pose and scale drift. To enhance depth accuracy further, we incorporate learned monocular depth priors. We propose a novel joint depth and scale adjustment (JDSA) module to solve the scale ambiguity inherent in depth priors. Extensive evaluations across synthetic and real-world datasets validate that our approach outperforms existing methods in accuracy and map completeness while preserving real-time performance.
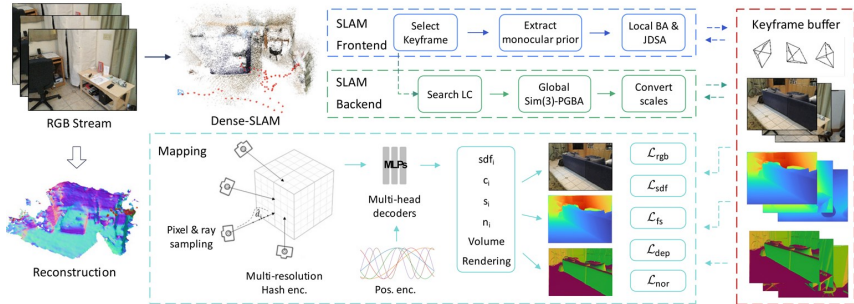
Figure 10: System overview: Given an RGB image stream, our system runs parallel tracking and mapping. On tracking part, two processes, namely frontend and backend, are spawn for local and global consistent tracking respectively. Our SLAM frontend further leverages a pre-trained CV model to predict monocular geometric priors. The keyframe data, including estimated poses, depths, and monocular normal priors, are shared between processes. On the mapping side, the neural map is constructed incrementally based on the latest estimates from the shared buffer in an online manner.
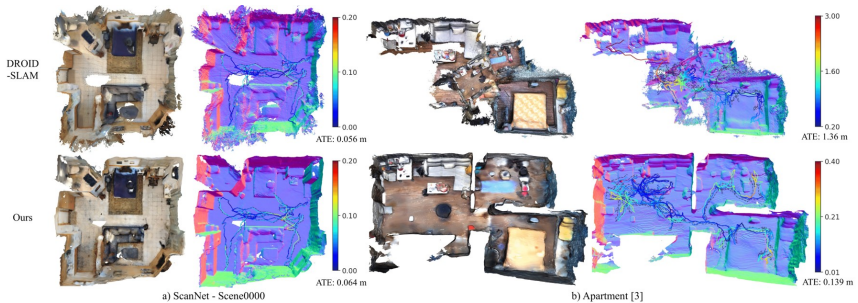

Figure 11: Qualitative results of reconstructed maps and estimated trajectories colored by ATE. Our method can produce more complete maps while using less memory footprint, object surfaces are smoother with finer details. On the apartment dataset, DROID-SLAM fails to detect all loop closures and suffers from severe scale drift.

Towards classification of LIDAR data involved with Bathymetry problems (L. Pournodrati)

Bathymetry, the measurement and mapping of underwater topography, plays a crucial role in various fields such as navigation, marine geology, and environmental monitoring. The study focuses on the development and evaluation of an innovative airborne LiDAR system designed to enhance efficiency and precision in bathymetric surveys. The system, equipped with advanced features including simultaneous green and infrared light emissions, enables precise delineation of water surface and seabed, particularly in shallow water regions and shoreline areas. Data analysis is facilitated through the recording and storage of full signal waveforms using high-speed analog-to-digital converters. Evaluation in real-world conditions demon-

strates the system's capability in generating high-resolution bathymetric datasets, showcasing its potential for improving underwater terrain mapping accuracy and efficiency. The findings of this study contribute to the ongoing advancements in airborne LiDAR bathymetry technology, analyzing new avenues for research and applications in marine science and geospatial studies. Modern full-waveform laser bathymetric scanners present a promising avenue for practical applications in airborne laser bathymetry (ALB) data algorithms, offering valuable insights into aquatic environments. The reliability and efficiency of classification algorithms depend on the selection of appropriate features. We focus on extracting important and efficient features from recorded signals and developing ideas for bathymetry data classification to overcome drawbacks of new captured data and correctly classify areas covered with vegetation which flows inside of the water.

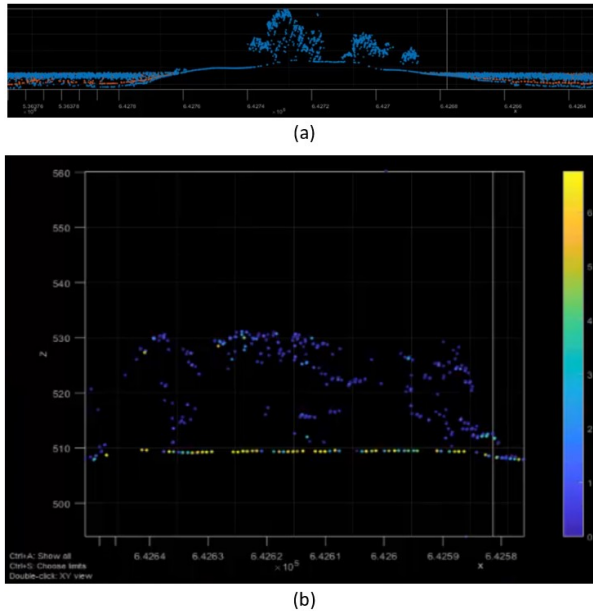Figure 12: Region of interest for analyzing.

(a)

(b)

Figure 13: (a) Raw point cloud. (b) Magnified view of area after preprocessing and initial classification.

References 2023

Burkhardt, M., Gienger, A., Joachim, L., Haala, N., Sörgel, U., Sawodny, O.: Data-based error compensation for georeferenced payload path tracking of automated tower cranes. Mechatronics, Vol 94.

Collmar, D., Walter, V., Kölle, M., Sörgel, U.: From multiple Polygons to single Geometry: Optimization of Polygon Integration for crowdsourced Data. ISPRS Annals of the Photogrammetry, Remote Sensing and Spatial Information Sciences, X-1/W1-2023, 159-166.

Collmar, D., Walter, V., Kölle, M., Sörgel, U.: A two-step approach for the acquisition of individual tree outlines using paid crowdsourcing, 43. Wissenschaftlich-Technische Jahrestagung der DGPF, 22.-23. März 2023 in München, 163-173.

Fritsch, D., Sörgel, U.: In memoriam Prof. Dr.-Ing. Dr. h.C. mult. Friedrich (Fritz) Ackermann 1929 - 2021. Geo-spatial Information Science, 1-2.

Haala, N., Kölle, M.: Automatische Interpretation von UAV-Punktwolken – Spielerei oder Praktischer Nutzen? DVW Schriftenreihe, 105, UAV 2023 - Geodaten nach Maß, 95–104.

Haala, N., Zhang, W., Joachim, L., Skuddis, D.: SLAM für die Echtzeit-Erfassung von Innenräumen. 22. Internationale Geodätische Woche Obergurgl 2022, 188–179.

Haala, N., Zhang, W., Joachim, L., Skuddis, D., Abolhasani, S., Schwieger, V., Sörgel, U.: Zum Potenzial von SLAM-Verfahren für geodätische Echtzeit-Messaufgaben. Allgemeine Vermessungsnachrichten (avn), 163–172.

Kölle, M., Walter, V., Schmohl, S., Sörgel, U.: Learning on the Edge: Benchmarking Active Learning for the semantic Segmentation of ALS Point Clouds. ISPRS Annals of the Photogrammetry, Remote Sensing and Spatial Information Sciences, X-1/W1-2023, 945-952.

Schneider, P. J., Yang, C.-H., Li, Y., Koppe, M., Sörgel, U., Pakzad, K., Rudolf, T.: Development of a Web Platform to visualize PS-INSAR Data in a Building Information Management System. ISPRS Annals of the Photogrammetry, Remote Sensing and Spatial Information Sciences, X-1/W1-2023, 869-873.

Xiang, M., Azimi, S., Bahmanyar, R., Sörgel, U., Reinartz, P.: Vehicle Occlusion Removal from single aerial Images using generative adversarial Networks. ISPRS Annals of the Photogrammetry, Remote Sensing and Spatial Information Sciences, X-1/W1-2023, 629-634.

Yang, B., Haala, N., Dong, Z.: Progress and perspectives of point cloud intelligence. Geo-spatial Information Science (2023), 1-17.

Zhang, W., Wang, S., Dong, X., Guo, R., Haala, N.: BAMF-SLAM: Bundle Adjusted Multi-Fisheye Visual-Inertial SLAM Using Recurrent Field Transforms. 2023 IEEE International Conference on Robotics and Automation (ICRA), 6232-6238.

Zhang, X., Lin, D., Xue, R., Sörgel, U.: Target-guided Learning for rare Class Segmentation in large-scale urban Point Clouds. The International Archives of the Photogrammetry, Remote Sensing and Spatial Information Sciences, XLVIII-1/W2-2023, 1693-1698.

Doctoral Theses

Kölle, M.: Forming a hybrid Intelligence System by Combining Active Learning and paid Crowdsourcing for semantic 3D Point Cloud Segmentation.

Schneider, P.: On the Analysis and Patterns of Persistent Scatterer Interferometry Results for Satellite-based Deformation Monitoring.

Master Theses

Buechner, L.: Estimating Canopy Traits from Hyperspectral Satellite Data using Convolutional Neural Networks. Supervisors: Coops, N. (The University of British Columbia, Faculty of Forestry), Miraglio, Z. (The University of British Columbia, Faculty of Forestry), Haala, N.

Cekic, A.: Albrecht Meydenbauers Karte von Freyburg/Unstrut - Genauigkeitsuntersuchung und historische Einordnung der ersten deutschen photogrammetrischen Geländeaufnahme. Supervisor: Cramer, M.

Hackstein, V.: Depth-Supervised Neural Surface Reconstruction from Airborne Imagery. Supervisors: Haala, N., Rothermel, M. (nFrames GmbH), Tutzauer, P. (nFrames GmbH).

Hu, J.: Quality of (photogrammetric) cameras – image resolution and the impact of image blur compensation. Supervisor: Cramer, M.

Lai, T.H.: A measuring system for determining the optical imaging quality of ADAS cameras. Supervisors: Huerland, A. (Daimler Sindelfingen), Meisterknecht, A. (Daimler Sindelfingen), Cramer, M.

Li, Y.: Development of a Web Platform for the Integration of DInSAR Deformation Measurements into Building Information Modeling. Supervisors: Schneider, P., Yang, C.H. (EFTAS), Sörgel, U.

Müller, H.: Investigation and Implementation of Fisheye Camera Models into Droid-SLAM. Supervisors: Zhang, W., Haala, N.

Sprügel, N.: Development of Feature Detection Based on Semantic Segmentation for Visual Odometry in Agricultural Environments. Supervisors: Haala, N., Moss, D. (Fraunhofer-Institut für Produktionstechnik und Automatisierung (IPA)).

Vincent, R.: Analysis and implementation of rotation-equivariant neural network architectures for feature extraction. Supervisors: Brändle, M. (MBDA Deutschland GmbH), Haala, N.

Bachelor Theses

Huang, K.: Deep-Learning based Building Detection in Rasterized 3D Airborne Laser Scanning Data. Supervisor: Laupheimer, D.

Rößle, J.: Integration und Analyse crowd-basierter Freihanderfassungen. Supervisors: Walter, V., Collmar, D., Kölle, M.

Ullmann, R.: Automatisierung von Crowdsourcing-Kampagnen inklusive qualitativer Auswertung am Beispiel von Microworkers.com. Supervisors: Walter, V., Collmar, D., Kölle, M.

Veser, E.: Untersuchungen zur radiometrischen Bildqualität von (photogrammetrischen) Kamerasystemen. Supervisor: Cramer, M.

Activities in National and International Organizations

Cramer, M.:

   Secretary German Society of Photogrammetry, Remote Sensing and Geoinformation (DGPF)
   Advisor ISPRS WG I/6: Orientation, Calibration and Validation of Sensors
   Member of DIN Normungsausschuss NA 005-03-02 AA "Photogrammetrie und Fernerkundung"

Englich, M.:

   Webmaster ISPRS

Haala, N.:

   Chair ISPRS WG II/2: Point Cloud Generation and Processing
   Chair EuroSDR Commission II: Modelling and Processing
   Vorsitz DGPF Arbeitskreis Sensorik und Plattformen

Sörgel, U.:

   President German Society for Photogrammetry, Remote Sensing and Geoinformation (DGPF)

Walter, V.:

   National Correspondent of the ISPRS Commission IV

Education - Lectures/Exercises

Bachelor "Geodäsie und Geoinformatik"

Geoinformatics I (Walter)	2/2
Geoinformatics II (Walter)	1/1
Image Processing (Haala)	2/1

Image Analysis (Haala, Cramer)	0/1
Integrated Fieldworks (Haala, Hobiger, Sneeuw)	0/4
Introduction into Geodesy and Geoinformatics (Cramer, Hobiger, Sneeuw, Sörgel)	2/2
Photogrammetry (Cramer)	2/1
Remote Sensing (Sörgel)	2/1
Urban Planning (Dvorak)	2/0

Master Course "Geodäsie und Geoinformatik"

Aerotriangulation (Cramer)	1/1
Computational Geometry (Walter)	1/1
Computer Vision for Image-based Acquisition of Geodata (Haala)	1/1
Databases and Geographical Information Systems (Walter)	1/1
Fundamentals in Urban Planning (Dvorak)	2/0
Modelling and Visualisation (Haala)	1/1
Pattern Recognition and Image Understanding (Sörgel, Haala)	1/1
Photogrammetric Acquisition of 3D Geodata (Cramer, Haala)	2/2
Project Geodesy and Geoinformatics (Haala)	4/2
Selected Chapters in Remote Sensing (Sörgel)	1/1
Signal Processing (Sörgel)	1/1
Simultaneous Localization and Mapping (SLAM) (Haala, Hobiger)	2/2
Web-based GIS (Walter)	1/1

Master Course GEOENGINE

Airborne Data Acquisition (Cramer)	2/1
Computer Vision (Haala)	2/1
Geoinformatics (Walter)	2/2
Integrated Fieldworks (Haala, Hobiger, Sneeuw)	0/4
Signal Processing (Sörgel)	2/1
Pattern Recognition (Sörgel)	2/1
Remote Sensing (Sörgel)	2/1

Master Course "Infrastructure Planning"

Introduction to GIS (Walter)	2/0

Master Course "Aerospace Engineering"

Image Processing (Haala)	2/1
Introduction to Projective Geometry (Cramer)	1/0